

**MEASUREMENT OF TRANSVERSE RELAXATION TIME (T2)  
OF IRON BY USING 1.5 T AND 3T MAGNETIC RESONANCE  
IMAGING ; A STUDY IN PHANTOM MODEL**

**WATCHAREE PRASERTKULCHAI**

**A THESIS SUBMITTED IN PARTIAL FULFILLMENT  
OF THE REQUIREMENTS FOR  
THE DEGREE OF MASTER OF SCIENCE  
( RADIOLOGICAL TECHNOLOGY)  
FACULTY OF GRADUATE STUDIES  
MAHIDOL UNIVERSITY  
2008**

**COPYRIGHT OF MAHIDOL UNIVERSITY**

Thesis

Entitled

**MEASUREMENT OF TRANSVERSE RELAXATION TIME (T<sub>2</sub>)  
OF IRON BY USING 1.5 T AND 3 T MAGNETIC RESONANCE  
IMAGING; A STUDY IN PHANTOM MODEL**

.....  
Miss. Watcharee Prasertkulchai  
Candidate

.....  
Asst. Prof. Napapong Pongnapang, Ph.D.  
Major Advisor

.....  
Asst. Prof. Sawwanee Asavaphatiboon,  
M.Sc.  
Co-Advisor

.....  
Prof. Banchong Mahaisavariya, M.D.  
Dean  
Faculty of Graduate Studies

.....  
Asst. Prof. Napapong Pongnapang,  
Ph.D.  
Chair  
Master of Science Programme in  
Radiological Technology  
Faculty of Medical Technology

Thesis

Entitled

**MEASUREMENT OF TRANSVERSE RELAXATION TIME (T2)  
OF IRON BY USING 1.5 T AND 3 T MAGNETIC RESONANCE  
IMAGING; A STUDY IN PHANTOM MODEL**

was submitted to the Faculty of Graduate Studies, Mahidol University  
for the degree of Master of Science (Radiological Technology)

on

November 18, 2008

.....  
Miss Watcharee Prasertkulchai  
Candidate

.....  
Siriporn nitjaphanich, M.D.  
Chair

.....  
Assoc. Prof. Manus Mongkolsuk, M.Sc.  
Member

.....  
Asst. Prof. Napapong Pongnapang, Ph.D.  
Member

.....  
Prof. Banchong Mahaisavariya, M.D.  
Dean  
Faculty of Graduate Studies  
Mahidol University

.....  
Assoc. Prof. Virapong Prachayasittikul,  
Ph.D.  
Dean  
Faculty of Medical Technology  
Mahidol University

## **ACKNOWLEDGEMENTS**

This thesis would not be accomplished if there are no valuable suggestions, extensive support and assistance from my major advisor, Asst. Prof. Dr. Napapong pongnapang and Asst. Prof. Sawwanee Asavaphatiboon. I sincerely thank them for their valuable advice and guidance in this research.

I wish to thank Dr. Siriporn nitjaphanich and Assoc. Prof. Manus Mongkolsuk for their kindness in examining the research instrument and providing suggestions for improvement, and who was the external examiner of the thesis defense.

I would like to thank AIMC center, Ramathibodi Hospital, and all staff in the AIMC for support on acquisition data.

Finally, I would like to thank my family from the deepest of my heart for their love and encouragement towards my study and project.

Watcharee Prasertkulchai

**MEASUREMENT OF TRANSVERSE RELAXATION TIME (T<sub>2</sub>) OF IRON USING 1.5T AND 3T MAGNETIC RESONANCE IMAGING; A STUDY IN PHANTOM MODEL****WATCHAREE PRASERTKULCHAI 4737561 MTRT/M****M.Sc. (RADIOLOGICAL TECHNOLOGY)****THESIS ADVISORS: NAPAPONG PONGNAPANG, Ph.D., SAWWANEE ASAVAPHATIBOON, M.Sc.****ABSTRACT**

Magnetic Resonance Imaging (MRI) is currently widely used as a diagnostic tool in medicine. Iron concentration in different organs such as heart and liver can be used to diagnose various diseases. The iron concentration in vivo can be measured by estimating transverse relaxation times (T<sub>2</sub>) and comparing the values with known different concentrations of iron in phantom model. This study was carried out to compare results of iron concentration measurements from 1.5T and 3.0T MRI systems. A General Electrics 1.5T and a Philips 3.0T MRI systems at AIMC center, Ramathibodi hospital were used in this study. Clinically relevant iron concentrations ranging from 0.3 mgFe to 45.3 mgFe were prepared in the phantom model. T<sub>2</sub> calculation was based on spin echo method. Technical settings were TR = 2500 msec, TE ranged from 6 msec to 126 msec, Field of view 350, matrix size 256 x 256 and slice thickness 6 mm with slice gap 6 mm. The results showed T<sub>2</sub> values ranged from 5.09 - 66.21 and 3.79 - 36.14 for 1.5T and 3.0T systems, respectively. Accuracy of measurement in terms of percentage error was found between 0.4% to 24% and 3% to 23% for 1.5T and 3.0T systems, respectively. We conclude that T<sub>2</sub> values and iron concentration were related exponentially. Moreover, in clinically relevant iron concentration level, T<sub>2</sub> values obtained from 1.5T system were about 35% longer than those from 3.0T system. Our study suggested that a calibration curve specific to each MRI system must be obtained.

**KEY WORDS: TRANSVERSE RELAXATION TIME / IRON / PHANTOM  
MODEL**

50 pp.

การวัดค่า T2 ของสารละลายเหล็กด้วยเครื่องสร้างภาพด้วยสนามแม่เหล็กที่มีความเข้มสนามแม่เหล็ก 1.5 เทสลา และ 3 เทสลา โดยศึกษาในแฟนทอม

( MEASUREMENT OF TRANSVERSE RELAXATION TIME (T2) OF IRON BY USING 1.5 T AND 3 T MAGNETIC RESONANCE IMAGING ; A STUDY IN PHANTOM MODEL )

วัชร ประเสริฐกุลชัย 4737561 MTRT/M

วท.ม.( รังสีเทคนิค )

คณะกรรมการควบคุมวิทยานิพนธ์ : นภาพงษ์ พงษ์นากค์, Ph.D. เสาวนีย์ อัสวาศดิบุญ, M.Sc.

#### บทคัดย่อ

ในปัจจุบันเครื่องสร้างภาพด้วยสนามแม่เหล็กไฟฟ้า(MRI)ได้นำมาใช้อย่างกว้างขวางในการวินิจฉัยโรคซึ่งจะมีความเข้มสนามแม่เหล็กที่ใช้กันอยู่ที่ 1.5 และ 3 เทสลา ได้มีการนำเครื่องสร้างภาพด้วยสนามแม่เหล็กไฟฟ้า (MRI) มาใช้ตรวจวัดหาปริมาณเหล็กในอวัยวะต่างๆ เช่น หัวใจและตับ เป็นต้น โดยหาค่าได้จากกราฟเปรียบเทียบ(Calibration curve) ของความสัมพันธ์ระหว่างค่าเวลาการคายพลังงานตามขวาง (T2 relaxation time) ซึ่งหาได้จากกราฟความสัมพันธ์ของค่าสัญญาณ (signal intensity) ของเหล็กกับค่า echo time ที่มีค่าต่างกัน และค่าความเข้มข้นของสารละลายเหล็กที่ทราบค่า ดังนั้นการศึกษาครั้งนี้ได้ทำการทดลองในแบบจำลอง เพื่อสร้างกราฟเปรียบเทียบ(Calibration curve) ของความสัมพันธ์ระหว่างค่า T2 ที่ได้จากการสร้างภาพด้วยสนามแม่เหล็กไฟฟ้า (MRI) และค่าความเข้มข้นของสารละลายเหล็กที่ทราบค่าในช่วง 0.3 – 45.3 มิลลิกรัมเหล็ก โดยทำการเก็บข้อมูลในเครื่องสร้างภาพด้วยสนามแม่เหล็กไฟฟ้า 1.5 และ 3.0 เทสลา ณ โรงพยาบาลรามารับดี ด้วยพารามิเตอร์ดังต่อไปนี้ TR = 2500 msec TE อยู่ในช่วง 6 msec ถึง 126 msec และใช้ขนาดภาพ (FOV) 350 มิลลิเมตร ที่มีความหนาของภาพ 6 มิลลิเมตรด้วยความละเอียด (Matrix) 256 x 256 จุด ที่เหมือนกัน จากการทดลอง พบว่าค่า T2 ในเครื่อง 1.5 เทสลา มีค่ามากกว่าในเครื่อง 3.0 เทสลาเฉลี่ยอยู่ที่ 35 เปอร์เซ็นต์ และเมื่อนำกราฟเปรียบเทียบที่ได้จากการทดลอง มาคำนวณหาค่าความเข้มข้นของเหล็กที่ไม่ทราบค่า พบว่าในเครื่อง 1.5 เทสลา มีเปอร์เซ็นต์ค่าความคลาดเคลื่อนต่ำสุด- สูงสุดเท่ากับ 0.4-24 % และสำหรับเครื่อง 3.0 เทสลา มีค่า เปอร์เซ็นต์ค่าความคลาดเคลื่อนต่ำสุด-สูงสุดเท่ากับ 3-22 % สรุปได้ว่ากราฟความสัมพันธ์ระหว่างค่าเวลาการคายพลังงานตามขวาง (T2 relaxation time)กับค่าความเข้มข้นของสารละลายเหล็กเป็นแบบเอ็กซ์โปเนนเชียลและค่าT2 ในเครื่อง 1.5 เทสลา มีค่ามากกว่าในเครื่อง 3.0 เทสลา

50 หน้า

## CONTENTS

	<b>Page</b>
<b>ACKNOWLEDGEMENTS</b>	iii
<b>ABSTRACT</b>	iv
<b>LIST OF TABLES</b>	vii
<b>LIST OF FIGURES</b>	viii
<b>LIST OF ABBREVIATIONS</b>	x
<b>CHAPTER</b>	
<b>I    INTRODUCTION</b>	<b>1</b>
<b>II   OBJECTIVES</b>	<b>13</b>
<b>III  LITERATURE REVIEWS</b>	<b>14</b>
<b>IV   MATERIALS AND METHODS</b>	
4.1   Materials	<b>18</b>
4.2   Methods	<b>23</b>
<b>V    RESULTS</b>	<b>28</b>
<b>VI   DISCUSSION</b>	<b>35</b>
<b>VII  CONCLUSIONS</b>	<b>37</b>
<b>REFERENCES</b>	<b>38</b>
<b>APPENDIX</b>	<b>41</b>
<b>BIOGRAPHY</b>	<b>50</b>

## LIST OF TABLES

<b>Table</b>	<b>Page</b>
1. Clinical Interest Categorization of Estimated Hepatic Iron Concentrations	15
2. The parameters were used in this study	23
3. The mean and SD of T2 values of manganese chloride (MnCl <sub>2</sub> ) solutions concentrations in 1.5 T MR scanner	28
4. The mean and SD of T2 values of manganese chloride (MnCl <sub>2</sub> ) solutions concentrations in 3.0T MR scanner	28
5. Percentage of error of calculated iron concentrations from the fitted equations of calibration curve in 1.5 T MR scanner	30
6. Percentage of error of calculated iron concentrations from the fitted equations of calibration curve in 3.0 T MR scanner	30
7. Percentage of error of calculated iron concentrations from the fitted equations of Figure 22 and 23 in 1.5 T MR scanner	32
8. Percentage of error of calculated iron concentrations from the fitted equations of Figure 24 and 25 in 3.0 T MR scanner	34



## LIST OF FIGURES

Figure	Page
1. Permanent Magnetic resonance Imaging Unit	2
2. These types of magnets are most often designed to produce a horizontal field due to their solenoid design	3
3. A vertical field Resistive Magnetic resonance Imaging Unit	3
4. Superconductive Magnetic resonance Imaging Unit	4
5a. In the absence of a strong magnetic field, hydrogen nuclei are randomly aligned as in , when the strong magnetic field, $\beta_o$ ,	6
5b. In the absence of a strong magnetic field, hydrogen nuclei are randomly aligned as in , applied, the hydrogen nuclei precess about the direction of the field	6
6a. The RF pulse, $\beta_{rf}$ , causes the net magnetic moment of the nuclei ,M, to tilt away from $\beta_o$	7
6b. When the RF pulse stops, the nuclei return to equilibrium such that M is gain parallel to $\beta_o$	7
7. Longitudinal relaxation is the return of longitudinal magnetization to equilibrium ( $B_0$ ) and is termed T1 recovery	9
8. Transverse relaxation is the return of transverse magnetization to equilibrium and is termed T2 decay	10
9. The spin echo signal and its dependence on TE	10
10. 3.0 Tesla superconductive magnetic resonance unit	18
11. 1.5 Tesla superconductive magnetic resonance unit	19
12. Torso Phase Arrays Coil for 3.0 T	19
13. Torso Phase Arrays Coil for 1.5T	20
14. ViewForum workstation of 3.0 T	20
15. Advantage workstation of 1.5 T	21

## LIST OF FIGURES (CONT.)

Figure	Page
16. The Acrylic cylinder Phantom with test tube	21
17. Acrylic cylinder phantom (Lateral view)	22
18. The curve between signal intensities and TE at each concentration	24
19. The relationship between T2 value and concentration of Iron (III) Chloride Hexahydrate ( $\text{FeCl}_3 \cdot 6\text{H}_2\text{O}$ ) solutions.	26
20. Graph showed the relationship between T2 values and concentrations of Iron (III) chloride solution in 1.5 T MR scanner	29
21. Graph showed the relationship between T2 values and concentrations of Iron (III) chloride solution in 3.0 T MR scanner	29
22. Graph showed the relationship between T2 values and concentrations of Iron (III) chloride solution ranged from 0.3 to 5.3 mg in 1.5 T MR scanner	31
23. Graph showed the relationship between T2 values and concentrations of Iron (III) chloride solution ranged from 10.3 to 45.3 mg in 1.5 T MR scanner	32
24. Graph showed the relationship between T2 values and concentrations of Iron (III) chloride solution ranged from 0.3 to 5.3 mg in 3.0 T MR scanner	33
25. Graph showed the relationship between T2 values and concentrations of Iron (III) chloride solution ranged from 10.3 to 45.3 mg in 3.0 T MR scanner	33
26. The curve relationship between signal intensities and echo times of manganese chloride solutions concentrations in 1.5 T	42
27. The curve relationship between signal intensities and echo times of manganese chloride solutions concentrations in 3.0 T	46

## LIST OF ABBREVIATIONS

Abbreviation	Term
AD	Alzheimer's disease
ADW	Advantage workstation
AIMC	Advanced Diagnostic Imaging and Image-Guided Minimal Invasive Therapy Center
$B_0$	The applied magnetic field
cm	Centimeter
cw	continuous wave
CSF	Cerebrospinal fluid
FDRI	The field-dependent R2 increase
FID	Free Induction Decay
FT	Fourier Transform
g	gram
GE	General Electric
GM	Gray Matter
HD	Huntington's disease
LIC	Liver Iron Concentrations
mgFe	milligram ferric
mm	Millimeter
mmol	Millimole
msec	Millisecond
MR	Magnetic Resonance
MRI	Magnetic Resonance Imaging
$M_{xy}$	Transverse Magnetization
NMR	Nuclear Magnetic Resonance
NMV	The net magnetic vector

**LIST OF ABBREVIATIONS (CONT.)**

<b>Abbreviation</b>	<b>Term</b>
PD	Parkinson's disease
R1	Longitudinal Relaxation Rate
R2	Transverse Relaxation Rate
RF	radio frequency
ROI	Region of Interest
SD	Standard deviation
SI	Signal Intensity
T	Tesla
T1	Longitudinal Relaxation time
T2	Transverse Relaxation time
TE	Echo Time
TR	Repetition Time
USA	The United States Of America
WM	White Matter
$\omega_0$	Larmor frequency
$\gamma$	The gyromagnetic ratio

## **CHAPTER I**

### **INTRODUCTION**

In the late 1940s, Felix Bloch and Edward Purcell independently developed methods for measuring the magnetic moments of nuclei in solid and liquid samples. By irradiating their samples with radiation to induce spin state transitions, they were able to calculate these magnetic moments by observing the subsequent dynamics of energy level transitions. This method is known as Nuclear Magnetic Resonance (NMR). Bloch and Purcell used continuous wave (cw) radiation in their NMR experiments, but most modern experiments used pulsed radiation to induce spin in a system of magnetic dipoles embedded in a solid or liquid. The process that is central to all NMR techniques is the detection and interpretation of the effects of such known perturbations applied to these systems. Unique magnetic behaviors such as spin relaxation times, which will be discussed in detail below, can be used to identify species in a test sample. The technique of magnetic resonance imaging (MRI) is used in modern medicine to produce three-dimensional images of portions of the body and aids doctors in diagnosing injuries<sup>(4)</sup>.

Clinical Magnetic Resonance Imaging (MRI) uses the magnetic properties of hydrogen and its interaction with both a large external magnetic field and radiowaves to produce highly detailed images of the human body. In this first module, we will discuss some basic principles of magnetism, the magnetic properties of the hydrogen nucleus, and its interaction with the externally applied magnetic field ( $B_0$ ). In its early days, MRI was known as NMR. This stands for Nuclear Magnetic Resonance. Although the name has changed (primarily due to the negative connotation of the word “nuclear”), the basic principles are the same. We derive our images from the magnetic resonance properties of nuclear particles (specifically hydrogen). In order to perform MRI, we first need a strong magnetic field. The field strength of the magnets used for MR is measured in units of Tesla. One Tesla is equal to 10,000 Gauss. The magnetic

field of the earth is approximately 0.5 Gauss. Given that relationship, a 1.0 T magnet has a magnetic field approximately 20,000 times stronger than that of the earth.

The type of magnets used for MR imaging usually belongs to one of three types; permanent, resistive, and superconductive. A permanent magnet is sometimes referred to as a vertical field magnet (Figure 1). These magnets are constructed of two magnets (one at each pole).



**Figure 1** Permanent Magnetic resonance Imaging Unit. <sup>(12)</sup>

The patient lies on a scanning table between these two plates. Advantages of these systems are: 1) Relatively low cost, 2) No electricity or cryogenic liquids are needed to maintain the magnetic field; 3) Their more open design may help alleviate some patient anxiety, 4) Nearly nonexistent fringe field. It should be noted that not all vertical field magnets are permanent magnets. Resistive magnets are constructed from a coil of wire. The more turns to the coil, and the more current in the coil, the higher the magnetic field. These types of magnets are most often designed to produce a horizontal field due to their solenoid design (Figure 2).

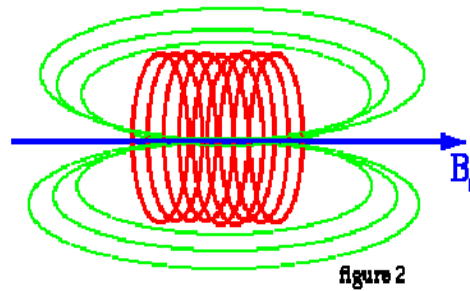


**Figure 2** These types of magnets are most often designed to produce a horizontal field due to their solenoid design <sup>(12)</sup>

As previously mentioned, some vertical field systems are based on resistive magnets (Figure 3). The main advantages of these types of magnets are 1) No liquid cryogen, 2) The ability to “turn off” the magnetic field, 3) relatively small fringe field. Below is an example of a vertical field resistive system.



**Figure 3** A vertical field Resistive Magnetic resonances Imaging Unit. <sup>(12)</sup>

Superconducting magnets are the most common. They are made from coils of wire (as are resistive magnets) and thus produce a horizontal field. They use liquid helium to keep the magnet wire at 4 degrees Kelvin where there is no resistance. The current flows through the wire without having to be connected to an external power source. The main advantage of superconducting magnets is their ability to attain field strengths of up to 3 Tesla for clinical imagers and up to 10 Tesla or more for small

bore spectroscopy magnets. Below is an example of a superconductive MR system (Figure 4).<sup>(12)</sup>



**Figure 4** Superconductive Magnetic resonance Imaging Unit.<sup>(12)</sup>

In order to understand MRI, it is necessary to understand the properties of atoms. Atoms consist of a dense nucleus surrounded by orbiting electrons. The nucleus of most atoms is made up of positively charged particles called protons, and neutrally charged particles called neutrons. The nucleus of an atom is always positively charged due to the positive protons. The electrons orbiting around the nucleus are extremely small negatively charged particles which balance the positive charge of the nucleus. Chemical properties of elements vary based on the electrical charge of the atoms. An atom with the same number of protons and electrons is chemically neutral and stable. Often, electrons are added or knocked out of the orbits around nuclei, which alters the charge of atom thus creating a positively or negatively charged particle. An atom which is positively or negatively charged is referred to as ionized. The simple nucleus of the hydrogen atom consists of one proton, and no neutrons. The hydrogen atom has a positive charge and an atomic number of 1 due to the presence of only one proton in its nucleus. For the purposes of MR, the hydrogen atom is referred to as a proton. The abundance of the hydrogen atoms in the human body, and the large magnetic moment (discussed below) created by the single proton in the nucleus of the atom, make hydrogen atoms extremely sensitive to magnetic resonance.



Based on these facts, we will concentrate on the hydrogen atom for the duration of this section. Hydrogen has the simplest atomic structure compared to all other elements. There is an abundance of hydrogen in the human body. Approximately 70% of the body is made up of water which contains two hydrogen atoms and one oxygen atom. It is the hydrogen atoms that are focused on to produce an MR image. The moving (spinning) hydrogen protons create a magnetic field, and thus perform as a tiny magnet with a north and a south pole. Since there are two magnetic poles, the protons are referred to magnet dipoles. Based on the laws of electromagnetism, any electrically charged particle which moves creates a magnetic field called a magnetic moment. This is the property that allows hydrogen protons to behave predictably within an external magnetic field. The motion or the "spin" of the hydrogen atoms can be described as a random combination of the spinning of a top, the spin of a bowling ball and the rotation of the earth around its axis. Understanding the magnetic moment of the hydrogen protons, will lead to an understanding of the alignment of the protons within a magnet.<sup>(13)</sup>

The basis of MRI is the directional magnetic field, or moment, associated with charged particles in motion. Nuclei containing an odd number of protons and/or neutrons have a characteristic motion or precession. Because nuclei are charged particles, this precession produces a small magnetic moment. When a human body is placed in a large magnetic field, many of the free hydrogen nuclei align themselves with the direction of the magnetic field (figure 5(a)). The nuclei precess about the magnetic field direction like gyroscopes. This behavior is termed Larmor precession.

The frequency of Larmor precession is proportional to the applied magnetic field strength as defined by the Larmor frequency,  $\omega_o$ . (equation 1)

$$\omega_o = \gamma B_o \quad (1)$$

Where the gyromagnetic ratio,  $\gamma$  and  $B_o$  is the strength of the applied magnetic field. The gyromagnetic ratio is a nuclei specific constant. (For hydrogen,  $\gamma=42.6$  MHz/ Tesla)

At 1.5 T the precessional frequency of hydrogen is 63.855 MHz (1.5 T x 42.57 MHz).

At 3.0 T the precessional frequency of hydrogen is 127.71 MHz (3.0 T x 42.57 MHz).

To obtain an MR image of an object, the object is placed in a uniform magnetic field,  $B_0$ , of between 1.5 to 3.0 Tesla. As a result, the object's hydrogen nuclei align with the magnetic field and create a net magnetic moment,  $M$ , parallel to  $B_0$ . This behavior is illustrated in Figure 5 (b).

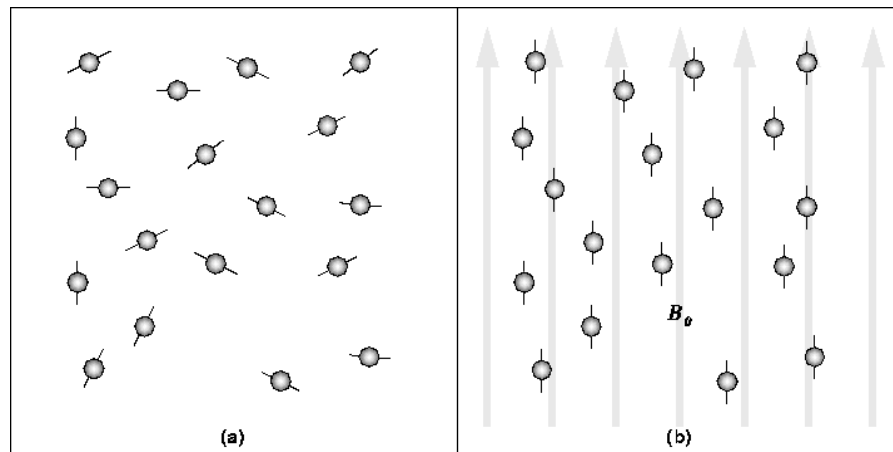


**Figure 5** In the absence of a strong magnetic field, hydrogen nuclei are randomly aligned as in (a). When the strong magnetic field,  $B_0$ , is applied, the hydrogen nuclei precess about the direction of the field as in (b). <sup>(24)</sup>

When a radio frequency (RF),  $B_{rf}$ , is applied perpendicular to  $B_0$ . This pulse, with a frequency equal to the Larmor frequency, causes  $M$  to tilt away from  $B_0$  as in Figure 6 (a). Resonance is referred to as the property of an atom to absorb energy only at the Larmor frequency. This is the basis of MR. An atom will only absorb external energy if that energy is delivered at precisely its resonant frequency. The energy must also be delivered at  $90^\circ$  to the net magnetic vector (NMV) and main magnetic field ( $B_0$ ). Otherwise, no energy will be absorbed, resonance will not have occurred and an image cannot be created. Excitation occurs when the proton absorbs the applied energy or resonates. As resonance occurs, the NMV moves out of alignment with the  $B_0$  to a pre-specified angle. The deflection of the magnetization or total angle created after the end of the RF pulse is referred to as the flip angle. When a  $90^\circ$  pulse is applied and the protons are given enough energy to be flipped into the x-y plane, the

net magnetization vector is now in the transverse plane.  $B_0$  or z-axis is now referred to as the longitudinal plane.

The protons are now rotating in the transverse plane at the Larmor frequency. As well as flipping into the transverse plane, the protons also begin rotating in phase with each other. When resonance occurs, the entire magnetic moments move into the same path or all flip the same number of degrees, and they all precess in phase with other. With the net magnetization in the transverse plane (created with a  $90^\circ$  flip angle), and a receiver coil or antenna in the transverse plane, a voltage is induced within the receiver coil. This oscillating signal voltage over time is the MR signal. The magnitude of the signal is dependent on the magnetization present in the transverse plane. At the termination of the RF, the freely precessing protons in the transverse plane ( $M_{xy}$ ) give up energy (RF) in order to try to realign with  $B_0$  (Figure 6 (b)). As the transverse magnetization starts to decay due to the loss of phase coherence, the protons eventually realign with  $B_0$ . This signal produced by the decay of transverse magnetization is called free induction decay (FID). The amplitude of the FID signal becomes smaller over time as net magnetization returns to equilibrium.

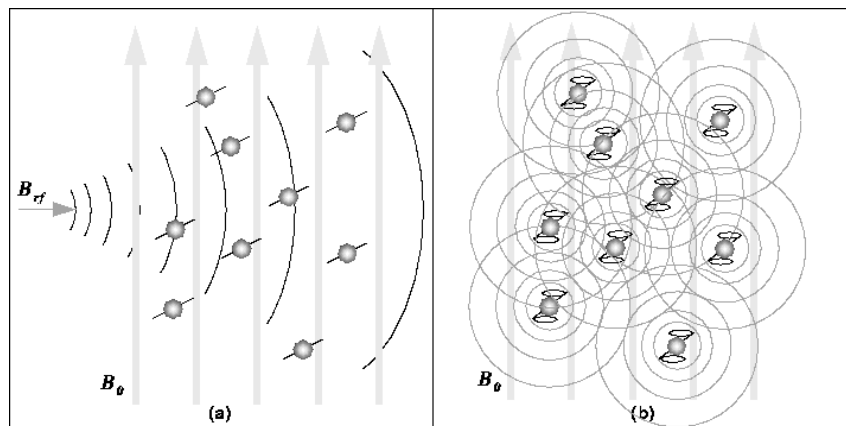


**Figure 6** (a) The RF pulse,  $B_{rf}$ , causes the net magnetic moment of the nuclei,  $M$ , to tilt away from  $B_0$ . (b) When the RF pulse stops, the nuclei return to equilibrium such that  $M$  is again parallel to  $B_0$ . During realignment, the nuclei lose energy and a measurable RF signal. <sup>(24)</sup>

When the RF pulse is terminated, the net magnetic vector (NMV) is once again influenced by the main magnetic field ( $B_0$ ) and tries to re-align with it along the longitudinal axis. Protons attempt to return from a state of non-equilibrium to a state of equilibrium. As the NMV gives up its absorbed RF energy while trying to return to  $B_0$ , the process of relaxation occurs. As relaxation is occurring, magnetization is recovering in the longitudinal plane while decaying in the transverse plane. The transverse magnetization induces a voltage in an antenna or receiver coil which will be eventually become the MR signal.

Relaxation combines 2 different mechanisms:

- Longitudinal relaxation corresponds to longitudinal magnetization recovery
- Transverse relaxation corresponds to transverse magnetization decay

Longitudinal and transverse relaxation times occur at simultaneously but are two completely different processes. Transverse magnetization decreases (T2 decay), while longitudinal magnetization increases (T1 recovery). Relaxation is a very important process in MR imaging as it determines the type of signal obtained greatly impacting the type of image generated.

Longitudinal relaxation is due to energy exchange between the spins and surrounding lattice (spin-lattice relaxation). As spins go from a high energy state back to a low energy state, RF energy is released back into the surrounding lattice. The longitudinal or spin-lattice relaxation time,  $T_1$  is the decay constant for the recovery of the  $z$  component of the nuclear spin magnetization,  $M_z$ , the recovery follows as equation 2.  $T_1$  is defined the decay constant for the recovery of  $M_z$  to return to 63% of its original length (Figure 7).

$$M_z = M_{z0} (1 - e^{-t/T_1}) \quad (2)$$

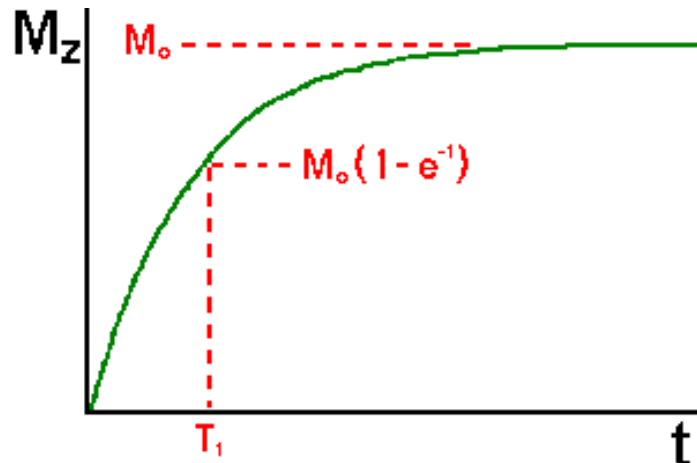


**Figure 7** Longitudinal relaxation is the return of longitudinal magnetization to equilibrium ( $B_0$ ) and is termed T1 recovery. <sup>(25)</sup>

Transverse relaxation or spin-spin relaxation time is the return of transverse magnetization to equilibrium. Although these two processes occur at the same time, they are quite different and thus contribute significantly different information to the resulting MR image. Unlike longitudinal relaxation, transverse relaxation is not a process of dissipation or absorption of energy into tissue. The decay of transverse magnetization is a process called T2 decay. As the amount of magnetization in the x-y (transverse) plane decreases, T2 decay increases. After an RF pulse, hydrogen nuclei are spinning in unison or in-phase with each other. As the magnetic fields of all the nuclei interact with each other, energy is exchanged between those nuclei. The nuclei which began spinning "in-phase" lose their phase coherence or dephase over time and spin in a random fashion. This process results in an exponential decrease or decay in transverse magnetization. Because T2 decay is the result of the exchange of energy between spinning hydrogen nuclei, it is referred to as "spin-spin" relaxation. The rate of T2 decay is also expressed as a time constant. T2 decay occurs when the transverse magnetization has decreased to 37% of its initial value (Figure 8). The time constant which describes the return to equilibrium of the transverse magnetization,  $M_{xy}$ , is called the spin-spin relaxation time, "T2". (1, 5, 6)

$$M_{xy} = M_{xy0} e^{-t/T2} \quad (3)$$

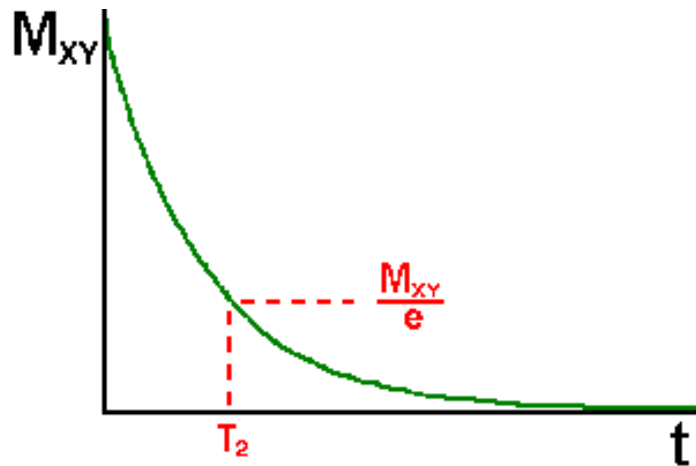


**Figure 8** Transverse relaxation is the return of transverse magnetization to equilibrium and is termed T2 decay. <sup>(25)</sup>

Transverse (T2) relaxation is the process in which the finite components of the magnetization present in the transverse plane decay to the zero (the equilibrium state). Often T2 relaxation is discussed in terms of two separate processes. One of these is driven by molecular movements and is known as “pure” T2 relaxation. The other is the result of the presence of a magnetic field gradient within the voxel of interest and is known as T2\* relaxation. To measure “pure” T2 relaxation independently of T2\* relaxation, spin echo acquisitions (Figure 9) are commonly used.

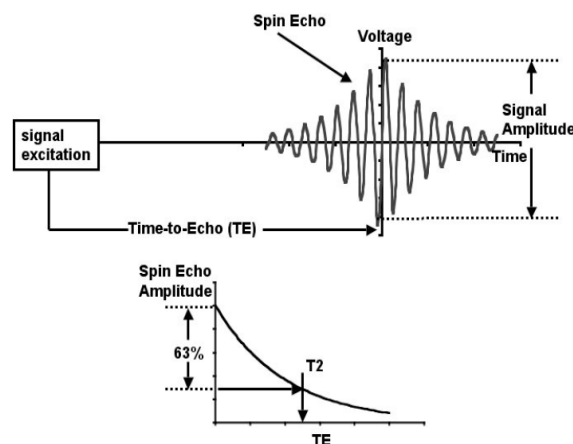


**Figure 9** The spin echo signal and its dependence on TE. <sup>(23)</sup>

The spin echo amplitude decays as the TE is lengthened as is illustrated in the graph provided in Figure 9. This is generally found to be described by a decaying exponential function which has a characteristic time constant. To determine the value of the characteristic time constant for transverse relaxation (T<sub>2</sub>) one finds the point at which 63% of the signal has decayed and then projects that point onto the TE axis.

Two factors contribute to the decay of transverse magnetization.

- 1) Molecular interactions (said to lead to a pure T<sub>2</sub> molecular effect)
- 2) Variations in B<sub>0</sub> (said to lead to an inhomogeneous T<sub>2</sub> effect)

The combination of these two factors is what actually results in the decay of transverse magnetization. The combined time constant is called T<sub>2</sub> star and is given the symbol “T<sub>2</sub>\*”. The relationship between the T<sub>2</sub> from molecular processes and that from inhomogeneities in the magnetic field is as follows.

$$1/T_2^* = 1/T_2 + 1/T_{2\text{inhomo}} \quad (4)$$

T<sub>2</sub> relaxation times may also be expressed as the relaxation rates R<sub>2</sub> = 1/T<sub>2</sub>. The 1/T<sub>2</sub> relaxation rate (R<sub>2</sub>) may be quantified using multiple echo sequences. If the decay of the net magnetization (M<sub>xy</sub>) is assumed to be mono-exponential, then R<sub>2</sub> is then given by

$$R_2 = \ln \left( \frac{SI(TE1)}{SI(TE2)} \right) / \Delta TE \quad (1)^{(16)}$$

Where SI (TE1) is the measured signal intensity at the first echo time(TE1) and SI(TE2) is the signal intensity at the second echo TE2 , respectively and ΔTE = (TE2 – TE1). The signal intensities (SI) can be measured from a region of interest (ROI), determined after the image obtained.

At the present, Magnetic resonance imaging (MRI) commonly uses for clinical diagnostic. It uses the magnetic properties of human body to provide pictures of any tissue. Hydrogen nuclei are a principal constituent of body tissues in water and lipid molecules. A hydrogen nucleus produces a dipole moment (magnetic field) that can interact with an external magnetic field. MRI machines generate a strong, homogeneous magnetic field by using a large magnet made by passing an electric field through super-conducting coils of wire. Patients placed in a horizontal cylinder are exposed to the magnetic field. Hydrogen nuclei in the body, which normally have randomly oriented spins, align in a direction parallel to the magnetic field. The MRI machine applies short electromagnetic pulses at a specific radio frequency (RF). The hydrogen nuclei absorb the RF energy and precess away from equilibrium. When the RF pulse is turned off, the precessing nuclei release the absorbed energy and return to the normal. The strength of the signal varies, depending on the applied RF magnetic fields. A tissue examined returns to normal occurs over characteristic curves called T1 and T2 relaxation time. The alteration of magnetization induces a voltage in an antenna or receiver coil which will be eventually become the MR signal.

For the measurement of the tissue iron concentration, MRI measures indirectly by detecting the effects on relaxation times of tissue storage iron (ferritin and haemosiderin) which are superparamagnetic. Because of the superparamagnetic and ferromagnetic properties of many forms of iron (with its unpaired electrons), iron compounds may have special effects on MRI. Both ferritin and haemosiderin have about 2000  $\text{Fe}^+$  ions per molecule and each ion has five unpaired electrons. Various types of iron result in subtle alterations in the local magnetic field environment of tissue protons. This, in turn, may cause enhanced relaxation with shortening of T1 or T2 relaxation times. Deposited iron concentration in tissues makes the rapidly dephasing of proton due to cause decreasing of T2 relaxation time. So the type and amount of shortening reflect the identity and quantity of the iron compounds present. As a result of the high sensitivity of MRI to various forms of iron, it has been said that iron is to MRI as calcium is to CT.<sup>(15)</sup>



## **CHAPTER II**

### **OBJECTIVES**

#### **Research Question:**

Are any relationships between Transverse relaxation times (T2) and Iron concentrations *in vitro* model?

#### **The Main objectives:**

- To assess correlation between T2 values and iron concentrations *in vitro* in order to create calibration curves for 1.5T and 3T MRI machines.
- To assess precision of calculated T2 value from calibration curves.
- To compare the difference of Transverse relaxation times (T2) between 1.5T and 3T.

### CHAPTER III

## LITERATURE REVIEWS

Iron is essential for virtually all living organisms. However, some forms of iron are potentially toxic to living cells. In most organisms, including humans, iron is stored in a relatively safe, oxidized state ( $\text{Fe}^{3+}$ ) within ferritin a hollow spherical protein shell 12 nm in diameter and capable of sequestering up to 4500 iron atoms in the form of ferrihydrite ( $5\text{Fe}_2\text{O}_3 \cdot 9\text{H}_2\text{O}$ ), which is mineralized in the protein's core. Iron is transported into the ferritin shell via three- and fourfold channel at the junctions of the protein's subunits. During this process, potentially toxic  $\text{Fe}^{2+}$  is oxidized for storage as ferrihydrite. In humans, abnormal accumulations of iron have been shown to be associated with many types of neurodegenerative diseases, such as Alzheimer's disease (AD), Parkinson's disease (PD) and Huntington's disease (HD) (Beard et al. 1993; Smith et al. 1997). Although this association was first discovered in AD tissue by Goodman in 1954 (Goodman 1953), the increase in iron does not appear to be related to an increase in levels of the ferritin protein or the iron transport protein transferrin (e.g. Beard et al. 1993).<sup>(5)</sup>

In 2003, H Pardoe, W Chua-anusorn<sup>1</sup>, TG St Pierre and J Dobson studied the detection limits for ferromagnetic particle concentrations using MRI-based  $R_2$  measurements. In their studies, they synthesized series of agar gel phantoms that contained known concentrations of ferrimagnetic material which were prepared in the presence of two types of polymer (dextran and polyvinyl alcohol) and performed in head coil of a Siemens Magnetom Vision 1.5T MRI scanner. They found that for both methods of particle preparation, concentrations of ferrimagnetic iron in agar gel less than  $0.01 \text{ mg ml}^{-1}$  had no measurable effect on the value of  $R_2$  for the gel. The results indicate that MRI-based  $R_2$  measurements using 1.5 T clinical scanners are not quite sensitive enough to detect the very low concentrations of nanoparticulate biogenic magnetite reported in human brain tissue.<sup>(9)</sup>

In 2004, Jose' M. Alu' stiza, MD and his research team evaluated the accuracy of magnetic resonance (MR) imaging in the quantification of hepatic iron concentration. Between April 1999 and June 2001, 112 patients were recruited prospectively. All had undergone liver biopsy and hepatic iron concentration quantification with spectrophotometry, followed by MR imaging. MR system was a 1.5T Gyroscan ACS-NT, Philips, Best, and Netherlands. Signal intensity (SI) was measured on images obtained with each sequence by means of regions of interest placed in the liver and paraspinal muscle to obtain the liver-to- ratio. The relationship between hepatic iron concentration and signal intensity ratio for each sequence was analyzed with multiple linear regressions. The study showed categorization of estimated hepatic iron concentrations fellow Table 1. They concluded that MR imaging is a very useful and noninvasive diagnostic tool that allows quantification of hepatic iron concentration in all possible levels of iron overload. <sup>(11)</sup>

<b>Iron Concentration</b>	<b>Category</b>
< 1.11 mgFe/g	Absence of iron overload
1.11 – 2.17 mgFe/g	Normal level or slight overload
2.23 – 4.41 mgFe/g	Moderate overload
> 4.44 mgFe/g	Very important overload; highly predictive of hemochromatosis

**Table 1** Clinical Interest Categorization of Estimated Hepatic Iron Concentrations.

In 2005, T G St. Pierre and team studied non-invasive measurement and imaging of tissue iron oxide nanoparticle concentrations in vivo using proton relaxometry. The presence of magnetic particles within tissue enhances the rate of dephasing of proton precession with higher concentrations of particles resulting in higher dephasing rates. Magnetic resonance imaging instruments can be used to measure and image the rate of decay of spin echo recoverable proton transverse magnetisation (R2) within tissues enabling the measurement and imaging of magnetic particle concentrations with the aid of suitable calibration curves. Applications include the non-invasive measurement of liver iron concentrations in iron overload disorders

and measurement and imaging of magnetic particle concentrations used in magnetic hyperthermia therapy. They have developed a method of measuring and imaging  $R_2$  within the liver. The method has a demonstrated dynamic range of measurement of liver iron concentration from 0.3 to 42.7 mg Fe/g dry liver tissue. The large dynamic range and sensitivity and specificity of liver  $R_2$  to needle biopsy measurements together with a demonstrated high degree of reproducibility on multiple magnetic resonance imaging units offers readily available non-invasive absolute liver iron concentration measurements to the clinical community.

The measurement of liver iron concentrations (LIC) is necessary for a range of iron loading disorders such as hereditary hemochromatosis, thalassemia, sickle cell disease, aplastic anemia, and myelodysplasia. Currently, chemical analysis of needle biopsy specimens is the most common accepted method of measurement. This study presents a readily available non-invasive method of measuring and imaging LIC in vivo using clinical 1.5 T magnetic resonance imaging units. Mean liver proton transverse relaxation rates ( $R_2$ ) were measured for 105 human subjects. A value for the LIC for each subject was obtained by chemical assay of a needle biopsy specimen. High degrees of sensitivity and specificity of  $R_2$  to biopsy LIC were found at the clinically significant LIC thresholds of 1.8, 3.2, 7.0 and 15.0 mg Fe/g dry tissue.<sup>(19)</sup>

A calibration curve relating liver  $R_2$  to LIC has been deduced from the data covering the range of LIC from 0.3 to 42.7 mg Fe/g dry tissue. Proton transverse relaxation rates in aqueous paramagnetic solutions were also measured on each magnetic resonance imaging unit to ensure instrument-independent results. Measurements of proton transverse relaxivity of aqueous  $MnCl_2$  phantoms on 13 different magnetic resonance imaging units using the method yielded a coefficient of variation of 2.1%.<sup>(19)</sup> and the one research from St.Pierre and team were applied Magnetic resonance imaging instruments can be used to measure and image the rate of decay of spin echo recoverable proton transverse magnetisation ( $R_2$ ) within tissues enabling the measurement and imaging of magnetic particle concentrations with the aid of suitable calibration curves.

Applications include the non-invasive measurement of liver iron concentrations in iron overload disorders and measurement and imaging of magnetic particle concentrations used in magnetic hyperthermia therapy. In this paper tell about

pathological iron oxide particles in tissue occur iron overload disorders such as thalassaemia and hereditary haemochromatosis affect up to 0.5% of the world's population. These disorders result in the accumulation of iron in the form of nanoparticles of iron (III) oxyhydroxide in organs of the body such as the liver, heart, spleen, and pancreas. Knowledge of the concentrations of these particles is often essential for appropriate management of iron overload conditions. The currently accepted and widely used method of measurement is chemical analysis of needle biopsy specimens of the liver. However, needle biopsy is an invasive procedure that carries a degree of risk and has associated sampling errors owing to the uneven distribution of iron within tissues. The method has a demonstrated dynamic range of measurement of liver iron concentration from 0.3 to 42.7 mg Fe/g dry liver tissue. The large dynamic range and sensitivity and specificity of liver R2 to needle biopsy measurements together with a demonstrated high degree of reproducibility on multiple magnetic resonance imaging units offers readily available non-invasive absolute liver iron concentration measurements to the clinical community.<sup>(20)</sup> In summary we will study any relationship T2 of iron between 1.5T and 3.0 T by using Iron(III) Chloride Hexahydrate ( $\text{FeCl}_3 \cdot 6\text{H}_2\text{O}$ ) solutions and comparison T2 value properties of iron between 3.0 T and 1.5 T.

## **CHAPTER IV**

### **MATERIALS AND METHODS**

The experiment was performed on 1.5 T and 3.0 T MRI units at AIMC, Queen Sirikits Building, Ramathibodi Hospital.

In this study, we acquired the images of each varied iron concentration at variable echo times on 1.5 T and 3.0 T MR scanners by using the following materials and methods.

#### **Materials**

1. Two Magnetic Resonance (MR) scanners were used in this study:

1.1 3.0 Tesla superconductive MR system (Achieva, Philips, Netherlands) was shown in Figure 10.



**Figure 10** 3.0 Tesla superconductive magnetic resonance unit

1.2 1.5 Tesla superconductive MR system (CV+NV/i, General Electric, USA) was shown in Figure 11.



**Figure 11** 1.5 Tesla superconductive magnetic resonance unit

## 2. Coils

Phase array coil was used for receiving signal from phantom which was transmitted radiofrequency pulse by body coil.

### 2.1 Torso Phase Array Coil for 3T MR system (Figure 12)



**Figure 12** Torso Phase Array Coil for 3T MR system

## 2.2 Torso Phase Array Coil for 1.5T MR system (Figure 13)



**Figure 13** Torso Phase Array Coil for 1.5T MR system

## 3. MR Workstation for measurement of MR signal intensities;

### 3.1 ViewForum workstation of 3.0 T MR system, software version 10.4 (Figure 14)

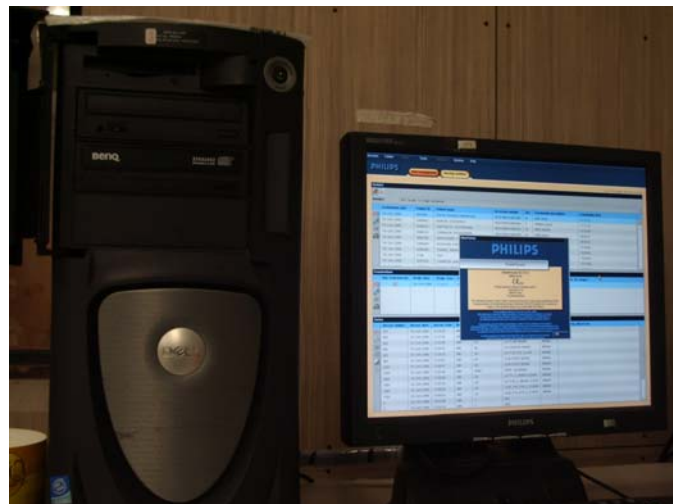


**Figure 14** ViewForum workstation of 3.0 T MR system



### 3.2 Advantage workstation of 1.5 T MR system, software version 4.1

(Figure 15)

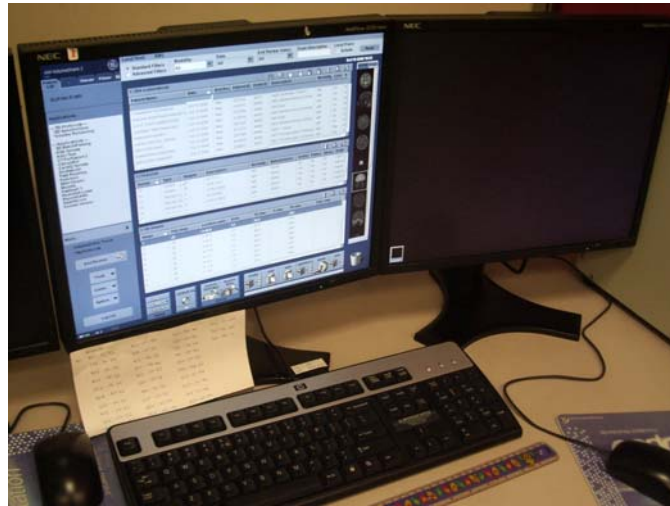


**Figure 15** Advantage workstation of 1.5 T MR system

#### 4. Phantom.

The phantom in this study was made of 9 inches in diameter cylindrical acrylic tube. Inside of a phantom was composed of ten glass tubes which were 17cc in volume for containing different solutions (Figure 16 and 17).

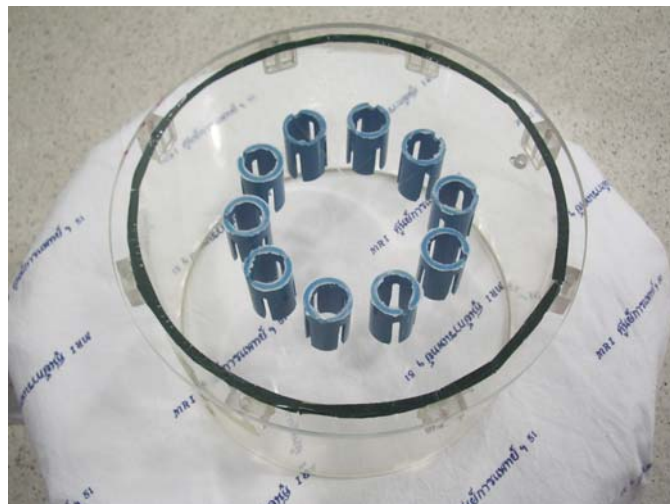


**Figure 16** The Cylindrical Acrylic phantom with ten glass tubes (Top view)



**Figure 17** The Cylindrical Acrylic phantom with ten glass tubes (Lateral view)

5. Manganese Chloride ( $\text{MnCl}_2$ ) solutions with varied concentration range from 0.2 to 3.4 mmol were used to test the reproducibility of T2 value.

6. Iron (III) Chloride Hexahydrate ( $\text{FeCl}_3 \cdot 6\text{H}_2\text{O}$ ) solutions with varied concentration of Iron from 0.3 to 45.3 mgFe were used to create the calibration curve.

## Methods

### 1. Quality control and reproducibility of T2 value

To ensure the quality of the MR scanner throughout the period of this experimental study, quality control of machines were preformed by the engineer. The reproducibility of T2 value is necessary to assess before acquiring the creation of calibration curve of iron concentration. Then we tested by using the following process in both 1.5 T and 3 T MR system:

1.1 Series of manganese chloride ( $\text{MnCl}_2$ ) solution varied concentration range from 0.2 mmol to 3.4 mmol (0.2, 0.6, 1.0, 1.4, 1.8, 2.2, 2.6, 3.0, 3.2, 3.4 mmol) were filled in each glass tube of the phantom. The volume surrounding these tubes was filled with saline water.

1.2 The phantom was positioned and properly leveled on the Torso phase array coil. The laser alignment light was used to position the phantom and set a landmark at the center of coil.

1.3 Performed the images of phantom by using the parameters following in the Table 2.

1.4 Repeated the scans five times in five days at the same parameters in both 1.5 T and 3.0 T MR scanner.

**Table 2** The parameters were used in this study

Parameter	1.5 Tesla (GE System)	3.0 Tesla (Philips System)
Coil	Torso phase array coil	Torso phase array coil
Plane	Axial	Axial
Pulse sequences	Spin echo	Spin echo
Repetition time (TR)	2500 ms	2500 ms
Echo time (TE)	range from 6 to 126 msec	Range from 6 to 126 msec
Inter echo time	10 msec	10 msec
Slicethickness	6 mm with slice gap 6 mm.	6 mm with slice gap 6 mm.
No.of slice	3 slices	3 slices
Field of view	350 mm.	350 mm.
Matrix size	256 x 256	256 x 256
Workstation Version	ADW 4.1	Viewforum 10.4

### 1.5 Data analysis of Reproducibility test of T2 value

1.5.1 At each of varied echo time (TE) image data, we measured and recorded signal intensity values of each concentration of manganese chloride ( $\text{MnCl}_2$ ) solutions by using region of interest (ROI) on workstation (For 1.5 T used ADW 4.1 and 3.0 T used Viewforum 10.4) which fixed the size of ROI  $0.3 \text{ cm}^2$ . Each concentration was measured randomly 3 times and averaged the signal intensity values.

1.5.2 Plotted the curve between signal intensities and TE of each concentration shown as Figure 18, and used the data from the curve to calculate T2 value following the equation 1.

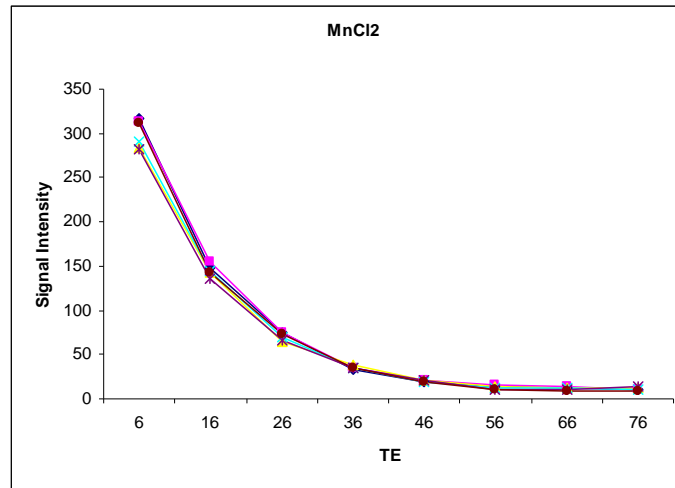


**Figure 18** The curve between signal intensities and TE at each concentration

$$T2 = \frac{(\Delta TE)}{\ln(SI(TE1) / SI(TE2))} \quad (\text{Equation 1})^{(1)}$$

SI (TE2) = Signal intensity at the 37% of SI (max)

SI (TE1) = Signal intensity at first echo time (msec)

$\Delta TE$  = TE (37% of SI (max)) – TE (1)

1.5.3 Repeated the steps of 1.5.1 and 1.5.2 on the other acquired image of each day.

1.5.4 Calculated the mean and standard deviation of T2 values of five day data.

## **2. Creation and Accuracy test of calibration curve of iron concentration.**

2.1 Creation of calibration curve of iron concentration which is the relationship between T2 values and variable iron concentrations. We acquired MR image of phantom by using the following process:

2.1.1 Prepared Iron (III) Chloride Hexahydrate ( $\text{FeCl}_3 \cdot 6\text{H}_2\text{O}$ ) solution with range from 0.3 mgFe/g to 45.3 mgFe/g (0.3, 5.3, 10.3, 15.3, 20.3, 25.3, 30.3, 35.3, 40.3, and 45.3) and filled in each glass tube of the phantom. The volume surrounding these tubes was filled with saline water.

2.1.2 The phantom was positioned and properly leveled on the Torso phase array coil. The laser alignment light was used to position the phantom and set a landmark at the center of coil.

2.1.3 Performed the images of phantom in 1.5 T and 3.0 T MR scanner by using the parameters in the Table 2.

### **2.1.4 Data analysis T2 value of iron**

2.1.4.1 At each of varied echo time (TE) image data, we measured and recorded signal intensity values of each concentration of Iron (III) Chloride Hexahydrate ( $\text{FeCl}_3 \cdot 6\text{H}_2\text{O}$ ) solutions by using region of interest (ROI) on workstation (For 1.5 T used ADW 4.1 and 3.0 T used Viewforum 10.4) which fixed the size of ROI  $0.3 \text{ cm}^2$ . Each concentration was measured randomly 5 times and averaged the signal intensity values.

2.1.4.2 Plotted the curve between signal intensities and TE of each concentration shown as Figure 18, and used the data from the curve to calculate T2 value of each concentration following the equation 1.

2.1.5 Plotted to create the calibration curve which is the relationship between T2 value and concentration of Iron (III) Chloride Hexahydrate ( $\text{FeCl}_3 \cdot 6\text{H}_2\text{O}$ ) solutions (Figure 19).

2.1.6 Fitted the proper equation of the calibration curve.

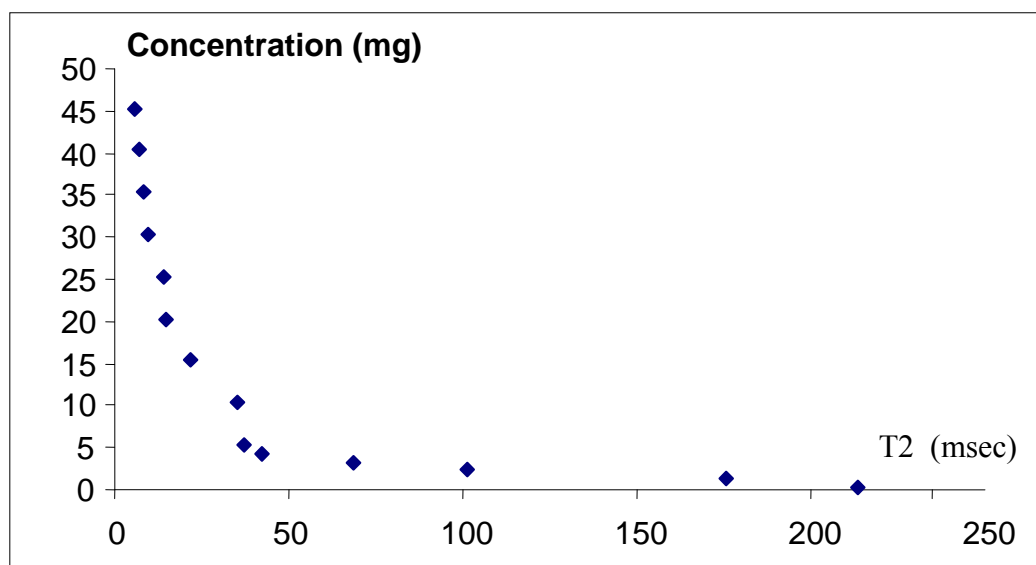


**Figure 19** The relationship between T2 value and concentration of Iron (III) Chloride Hexahydrate ( $\text{FeCl}_3 \cdot 6\text{H}_2\text{O}$ ) solutions.

2.2 Verification of the accuracy of calibration curves in this study; we assessed the unknown concentration of Iron (III) Chloride Hexahydrate ( $\text{FeCl}_3 \cdot 6\text{H}_2\text{O}$ ) solution from the curves by the following steps:

2.2.1 Prepared multiple unknown concentrations of Iron (III) Chloride Hexahydrate ( $\text{FeCl}_3 \cdot 6\text{H}_2\text{O}$ ) solutions and filled in the glass tubes of phantom.

2.2.2 Put the phantom on the Torso phase array coil properly and positioned it to the center of gantry. Then the images were acquired by using the parameters in Table 2 in both 1.5 T and 3.0 T MR scanner.

2.2.3 At each of varied echo time (TE) image data, we measured and recorded signal intensity values of each unknown concentration of Iron (III) Chloride Hexahydrate ( $\text{FeCl}_3 \cdot 6\text{H}_2\text{O}$ ) solutions by using region of interest (ROI) on workstation (For 1.5 T used ADW 4.1 and 3.0 T used Viewforum 10.4) which fixed the size of ROI  $0.3 \text{ cm}^2$ . Each concentration was measured randomly 5 times and averaged the signal intensity values.

2.2.4 Plotted the curve between signal intensities and TE of each unknown concentration shown as Figure 18, and used the data from the curve to calculate T2 value of each concentration following the equation 1.

2.2.5 Using the calculated T2 values from 2.2.4 to find Iron concentration from the fitted equation of the calibration curve in 2.1.6

2.2.6 Compared the calculated unknown Iron concentration with the true value and calculated the percentage of error.

## CHAPTER V

### RESULTS

#### 1. Reproducibility test of T2 value

In this study, the assessment of reproducibility of T2 value was done by finding mean and standard deviation (SD) of calculated T2 values from the graph which is the relationship between signal intensities and echo times at each concentration of MnCl<sub>2</sub> solutions (Appendix I). The results of mean and SD in 1.5T and 3.0T MR scanners were shown in Table 3 and 4, respectively.

**Table 3** The mean and SD of T2 values of manganese chloride (MnCl<sub>2</sub>) solutions in 1.5 T MR scanner

(MnCl <sub>2</sub> ) concentrations (mmol)	Mean T2	SD
0.2	66.21	± 2.06
0.6	23.75	± 1.33
1.0	13.71	± 0.19
1.4	9.64	± 0.33
1.8	7.50	± 0.26
2.2	6.05	± 0.14
2.6	5.55	± 0.20
3.0	4.67	± 0.18
3.2	5.12	± 0.14
3.4	5.09	± 0.36

**Table 4** The mean and SD of T2 values of manganese chloride (MnCl<sub>2</sub>) solutions in 3.0 T MR scanner

(MnCl <sub>2</sub> ) concentrations (mmol)	Mean T2	SD
0.2	36.14	± 2.37
0.6	12.96	± 0.71
1.0	9.21	± 0.70
1.4	6.49	± 0.25
1.8	4.63	± 0.33
2.2	3.88	± 0.34
2.6	3.81	± 0.38
3.0	3.91	± 0.35
3.2	3.90	± 0.48
3.4	3.79	± 0.20



## 2. Calibration curves and Accuracy test in 1.5 T and 3.0 T MR Scanners

The calibration curves of iron concentrations which was the relationship between T2 values and iron concentrations (mg) in 1.5T and 3.0T MR scanners were shown in Figure 20 and 21, respectively.

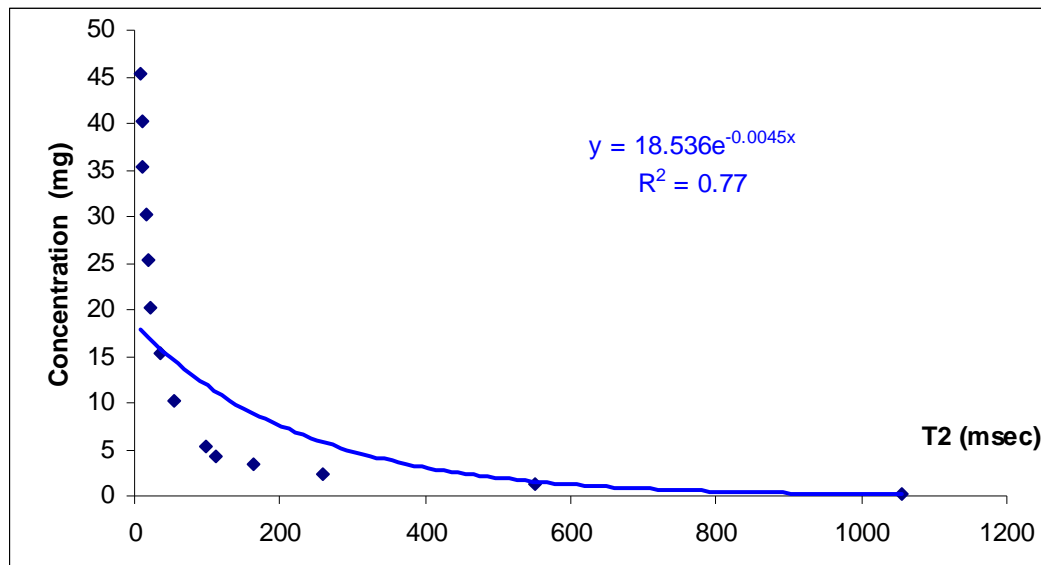


**Figure 20** Graph showed the relationship between T2 values and concentrations of Iron (III) chloride solution in 1.5 T MR scanner

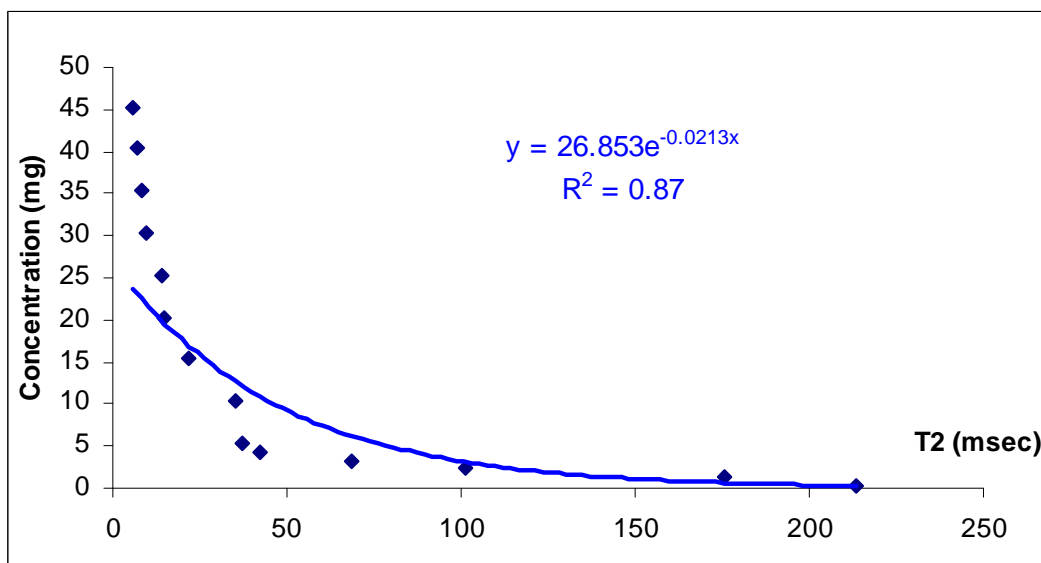


**Figure 21** Graph showed the relationship between T2 values and concentrations of Iron (III) chloride solution in 3.0T MR scanner

From Figure 20 and 21, the fitted equation of calibration curve in 1.5T was  $y = 18.536e^{-0.0045x}$  with  $R^2 = 0.77$  and in 3.0T was  $y = 26.853e^{-0.0213x}$  with  $R^2 = 0.87$ . When we used these equations to calculate the iron concentration of unknown solutions in 1.5 T and 3.0T MR scanners, the results of percentage of error were shown in Table 5 and 6, respectively. In 1.5T MR scanner, the minimum percent error was 3.86 % and the maximum percent error was 85.03 %. In 3.0T MR scanner, the minimum percent error was 3.57 % and the maximum percent error was 92.47 %.

**Table 5** Percentage of error of calculated iron concentrations from the fitted equations of calibration curve in 1.5 T MR scanner (Figure 20)

Iron Concentration (mgFe/g)	Iron Concentration Calculate (mgFe/g)	% error
3	5.55	85.03
6	10.87	81.27
9	14.09	56.65
12	14.47	20.59
15	15.58	3.86
18	16.27	-9.59
21	16.39	-21.92
24	16.54	-31.08
30	17.17	-42.74

**Table 6** Percentage of error of calculated iron concentration from the fitted equation of calibration curve in 3.0T MR scanner (Figure 21)

Iron Concentration (mgFe/g)	Iron Concentration Calculate (mgFe/g)	% error
3	4.02	34.09
6	11.54	92.47
9	11.84	31.56
12	14.60	21.72
15	16.62	10.82
18	18.64	3.57
21	19.83	-5.52
24	20.14	-16.04
30	22.04	-26.50

To fit the proper equation for calculation, the calibration curve was separated into two ranges of concentrations; 0.3-5.3 mg and 10.3-45.3 mg. For 1.5T MR scanner, the graphs were shown in Figure 22 and 23, respectively. The fitted equation of 0.3-5.3 mg was  $y = 5.7676 e^{-0.0028x}$  with  $R^2 = 0.98$  and the fitted equation of 10.3-45.3 mg was  $y = 49.038 e^{-0.0307x}$  with  $R^2 = 0.93$ . The result of calculated iron concentration of unknown solutions was shown in Table 7. The minimum percent error was -0.04 % and the maximum percent error was -25.12 %.

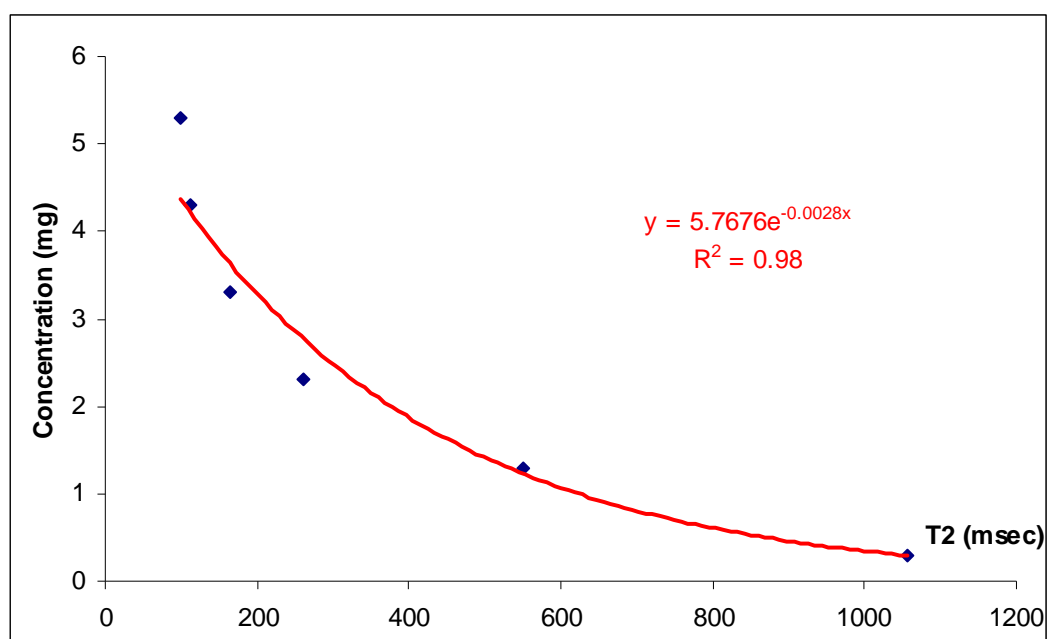


**Figure 22** Graph showed the relationship between T2 values and concentrations of Iron (III) chloride solution ranged from 0.3 to 5.3 mg in 1.5 T MR scanner

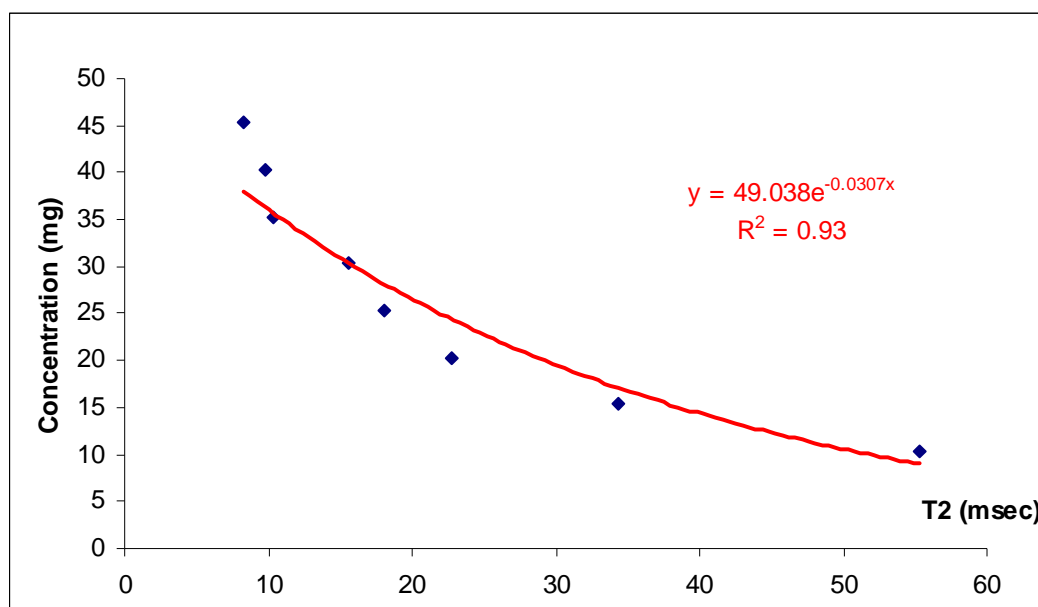


**Figure 23** Graph showed the relationship between T2 values and concentrations of Iron (III) chloride solution ranged from 10.3 to 45.3 mg in 1.5 T MR scanner

**Table 7** Percentage of error of calculated iron concentrations from the fitted equations of Figure 22 and 23 in 1.5 T MR scanner

Iron Concentration (mgFe/g)	Iron Concentration Calculate (mgFe/g)	% error
3	2.72	-9.20
6	4.49	-25.12
9	7.58	-15.75
12	9.05	-24.52
15	14.99	-0.04
18	20.17	12.10
21	21.22	1.08
24	22.54	-6.05
30	29.17	-2.74

For 3.0T MR scanner, the graphs were shown in Figure 24 and 25, respectively. The fitted equation of 0.3-5.3 mg was  $y = 8.807 e^{-0.0138x}$  with  $R^2 = 0.91$  and the fitted equation of 10.3-45.3 mg was  $y = 52.535 e^{-0.0505x}$  with  $R^2 = 0.93$ . The result of calculated iron concentration of unknown solutions was shown in Table 8. The minimum percent error was 3.35 % and the maximum percent error was 22.87 %.

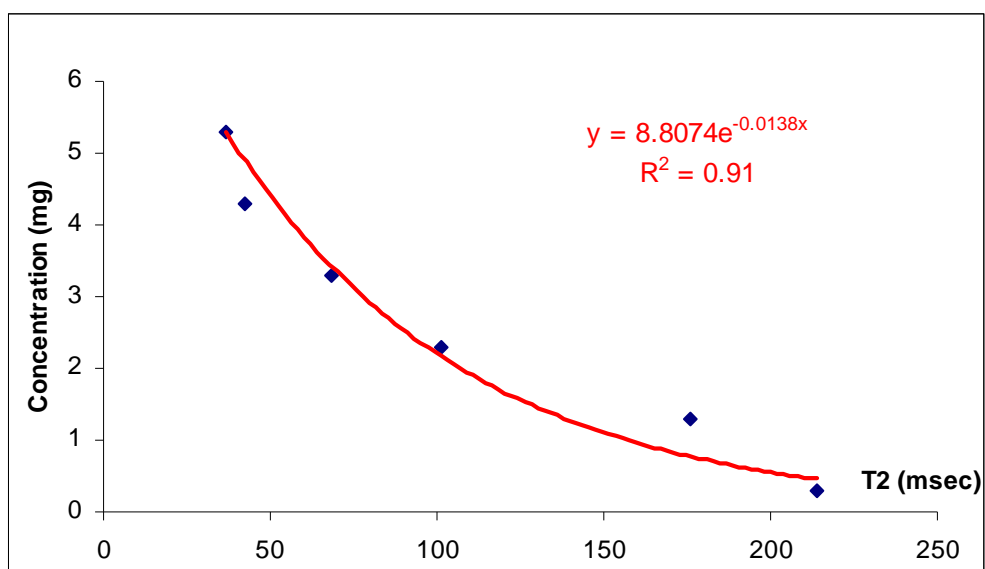


**Figure 24** Graph showed the relationship between T2 values and concentrations of Iron (III) chloride solution ranged from 0.3 to 5.3 mg in 3.0 T MR scanner

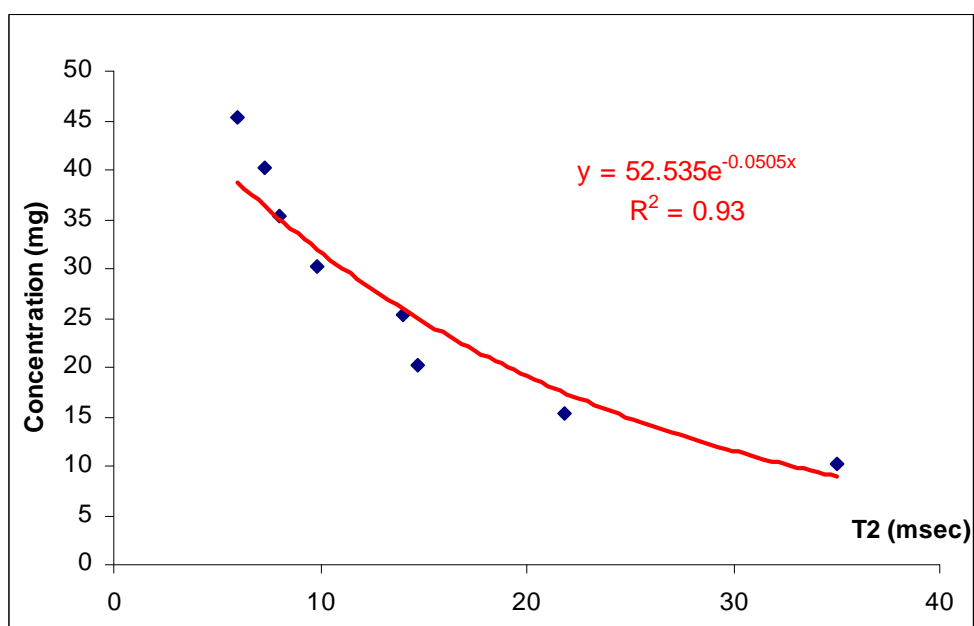


**Figure 25** Graph showed the relationship between T2 values and concentrations of Iron (III) chloride solution ranged from 10.3 to 45.3 mg in 3.0 T MR scanner

**Table 8** Percentage of error of calculated iron concentrations from the fitted equations of Figure 24 and 25 in 3.0 T MR scanner

Iron Concentration (mgFe/g)	Iron Concentration Calculate (mgFe/g)	% error
3	2.57	-14.18
6	5.09	-15.02
9	7.53	-16.23
12	12.40	3.35
15	16.85	12.36
18	22.11	22.87
21	25.63	22.04
24	26.59	10.79
30	32.92	9.74

## CHAPTER VI

### DISCUSSIONS

From Table 3 and 4 showed standard deviation (SD) of the T2 values for reproducibility test in 1.5T and 3.0T MR scanners. The minimum SD of T2 value was  $\pm 0.14$  in 1.5T and  $\pm 0.20$  in 3.0T. The maximum SD of T2 value was  $\pm 2.06$  in 1.5T and  $\pm 2.37$  in 3.0 T. In general the acceptable SD value is  $\pm 5$ . Then we concluded that the reproducibility of T2 value in both 1.5T and 3.0T MR scanners were acceptable.

Figure 20 and 21 showed the calibration curves and the fitted equations for 1.5T and 3.0T MR scanners. When using these equations to calculated iron concentration of unknown solutions (Table 5 and 6), the results were found that the maximum percentage of errors were very high in both systems. In 1.5T MR scanner, the percent error of calculated iron concentration of unknown solution with range 3-15 mgFe/g were overestimated and the others were underestimated. The minimum percent error was 3.86% and the maximum percent error was 85.03%. In 3.0 T MR scanner, the percent error of calculated iron concentration of unknown solution with range 3-18 mgFe/g were overestimated and the others were underestimated. The minimum percent error was 3.57% and the maximum percent error was 92.47%. We discussed that these errors came from the improper varied steps of range of iron concentrations and the errors from image acquisition and analysis of image data. It should increase more variable steps of iron concentrations especially range 0-5 mgFe/g because it was the range of Categorization of Estimated Hepatic Iron Concentrations (Table 1 in chapter 3).

From Figure 22-25, the calibration curve was separated into two ranges; 0.3-5.3 mgFe/g and 10.3-45.3 mgFe/g. The results of percentage of errors of calculated iron concentrations in both MR systems are better than the previous. In 1.5T MR scanner, the minimum percent error was -0.04% and the maximum percent error was -25.12%. In 3.0T MR scanner, the minimum percent error was 3.35% and the

maximum percent error was 22.87%. The percent errors of calculated iron concentration of unknown solutions were underestimated at the range  $< 10 \text{ mgFe/g}$  in both MR system. The percent errors in some concentrations were more than  $\pm 20\%$ .

In this study, T2 values in 1.5T were longer than 3.0T about 35%. Theoretical, more field strength induces more susceptibility effect, and then T2 value in high field strength is shorter than low field strength. The difference of the correlation between T2 values and iron concentration in 1.5T and 3.0T MR scanners cannot identify, but they are corresponding. Iron concentrations increase, T2 values decrease. Their relationships are exponential decay curves. We found that the measurement of T2 in MRI are affected by the instrument model, the applied field strength, the repetition and echo time used in the imaging sequence, the method used to analyze the relaxation curves, and other technical aspects of the measurement procedure including human error. So comparison of absolute signal intensities from one MRI unit to another is unreliable because of substantial inter machine variation.



## **CHAPTER VII**

### **CONCLUSIONS**

This vitro study demonstrates the good correlation between T2 values and iron concentrations in both 1.5T and 3.0T MR scanners. The T2 values of iron solutions in 1.5T are longer than 3.0T about 35%. We conclude that the measurement of T2 values in MRI can be used for estimation of the iron concentration or level.

The limitations of this study are the different model of MR scanners and the setting of scan parameters. Some parameters especially echo time (TE) cannot be adjusted to the suitable values including the problem of the appropriate varied step of iron concentration ranges.

Further study, we suggest that the study should vary more steps of lower range of iron concentrations and increase number and size of glass tube in the phantom.

## REFERENCES

1. Andrzej Cieszanowski, Wojciech Szeszkowski. Differentiation of focal hepatic lesion in Mr imaging with the use of combined quantitative and qualitative analysis. *Pol J Radiol* 2007; 72(1):26-35.
2. Badman, G. M. B. a. D. G. Noninvasive measurement of iron. *The American Society of Hematology* 2003; 101:15-19.
3. Craig K. Jones. T2 Decay Curve Acquisition and Analysis in MRI [online] 2003 [cited 2008 Nov 9] :1-3 Available from URL: <http://www.imaging.robarts.ca/~cjones/education/phd/thesis.pdf>
4. Colette Grabill , Afonso C. Silva , Sophia S. Smith , Alan P. Koretsky , Tracey A. Rouault. M RI detection of ferritin iron overload and associated neuronal pathology in iron regulatory protein-2 knockout mice. *Brain Research* 2003 ; 971:95–106.
5. D. Hautot, Q. A. P., N. Khan and J. Dobson. Preliminary evaluation of nanoscale biogenic magnetite in Alzheimer's disease brain tissue. *Proc. R.Soc.Lond.B (Suppl.)* 2003; 270:s62-s64.
6. D. Tyler, L. Marciani, P. Gowland. Accurate Imaging Measurement of T2 from a Single Echo Train. *Proc. Intl. Sot. Mag. Reson. Med* 2000; 8.
7. Dante Gatteschi, Roberta Sessoli and Andrea Cornia. Single-molecule magnets based on iron(III) oxo clusters. *Chem. Commun* 2000:725–732.
8. H. Dahnke, R. Bachmann, W. L. Heindel, C. Bremer, T. Schaefter. Fast T2\* mapping with SENSE acquisition and field inhomogeneity correction for lesion characterization and sensitive SPIO detection at 3.0T. *Proc. Intl. Soc. Mag. Reson. Med* 2005; 13:2205.
9. H Pardoe, W Chua-anusorn<sup>1</sup>, TGSt Pierre and J Dobson. Detection limits for ferrimagnetic particle concentrations using magnetic resonance imaging based proton transverse relaxation rate measurements. *Phys. Med. Biol* 2003; 48:N89–N95.

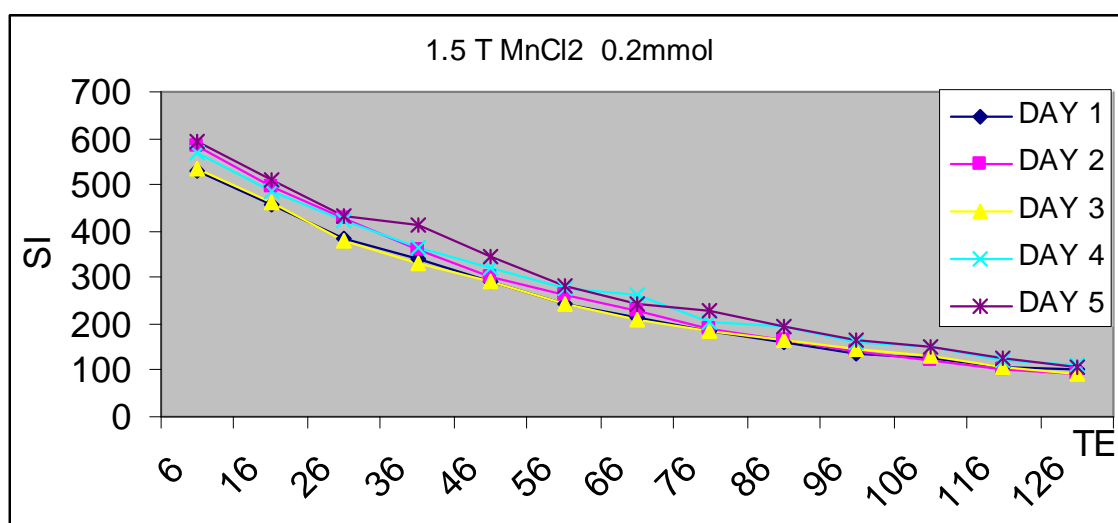
10. John C Wood, Cathleen Enriquez, Nilesh Ghugre , J. Michael Tyzka , Susan Carson, Marvin D Nelson and Thomas D Coates. MRI R2 and R2\* Mapping Accurately Estimates Hepatic Iron Concentration in Transfusion-Dependent Thalassemia and Sickle-Cell Disease Patients. Am Soc of Hematology 2004.
11. Jose´ M. Alu´ stiza, MD Jose´ Artetxe, MD Agustín Castiella, MD, Cristina Agirre, MD. MR Quantification of Hepatic Iron Concentration. Radiology 2004;230(2):479-484.
12. Kenneth P Batts. Iron overload syndromes and the liver. Modern Pathology 2007; 20:S31–S39.
13. Michael J. Childress. Pulsed Nuclear Magnetic Resonance : MIT Department of Physics 2003:1-4.
14. M Layrisse, C Martinez-Torres, M Renzy and I Leets. Ferritin iron absorption in Man. Blood 1975 May;45(5).
15. Paul Tofts. Quantitative MRI of the Brain measuring changes caused by disease. London: John Wiley&Sons; 2003.
16. Peter-D.Jensen. Evaluation of iron overload. British Journal of Haematology 2004; 124(6):697–711.
17. Robert Frazier. The Measurement of relaxation times in mineral oil and glycerin using pulsed nuclear magnetic resonance [online] 2005 [cited 2008 Nov 9]: 1-9 Available from URL: [http://physics.ucsd.edu/neurophysics/courses/physics\\_173\\_273/pulsed\\_NMR\\_heme.pdf](http://physics.ucsd.edu/neurophysics/courses/physics_173_273/pulsed_NMR_heme.pdf)
18. Serena J. Counsell, Nigel L. Kennea, Amy H. Herlihy, Joanna M. Allsop, Michael C. Harrison, Frances M. Cowan, Joseph V. Hajnal, Bridget Edwards, A. David Edwards, and Mary A. Rutherford. T2 Relaxation Values in the Developing Preterm Brain Am J Neuroradiol 2003 Sep; 24:1654–1660.
19. Timothy G. St. Pierre, P. R. C., Wanida Chua-anusorn, Adam J. Fleming, Gary P. Jeffrey, John K. Olynyk, Pensri Pootrakul, Erin Robins, and Robert Lindeman. Noninvasive measurement and imaging of liver iron concentrations using proton magnetic resonance. The American Society of Hematology 2005;105: 855-861.

20. T G St Pierre, P R Clark, W Chua-anusorn, A Fleming, H Pardoe, G P Jeffrey, J K Olynyk, P Pootrakul, S Jones, P Moroz. Non-invasive measurement and imaging of tissue iron oxide nanoparticle concentrations in vivo using proton relaxometry. *Journal of Physics* 2005; 7:122–126.
21. Vymazal J., Brooks, R.A., Bulte, J.W., Gadon, D & Aisen, P. Iron uptake By ferritin NMR relaxometry studies at low iron loads. *Journal of Inorganic Biochemistry* 1998; 71:153-157.
22. William G Bradley. FUNDAMENTALS OF MRI: Part II [online] 1998 [cited 2008 Nov 9] Available from URL : [http://www.e-radiography.net/mrict / fund%20mr2/fundmri%202.htm](http://www.e-radiography.net/mrict/fund%20mr2/fundmri%202.htm)
23. Wm. Faulkner. Basic Principles of MRI [ online ] 1996 [ cited 2008 Nov 9 ]: 1-16 Available from URL : [http://www.e-radiography.net/mrict/Basic\\_MR.pdf](http://www.e-radiography.net/mrict/Basic_MR.pdf).
24. B. Mackiewicz. Intracranial Boundary Detection and Radio Frequency Correction in Magnetic Resonance Images [ online ] 1995 [ cited 2008 Nov 9 ] Available from URL : [http:// www.cs.sfu.ca/~stella/ papers/blairthesis/main/node11.html](http://www.cs.sfu.ca/~stella/papers/blairthesis/main/node11.html).
25. Joseph P.Hornak. The Basics of NMR [ online ] 1997 [ cited 2008 Nov 9 ] Available from URL : <http://www.cis.rit.edu/htbooks/nmr/>
- 26 Yasuko Abe, Yasuyuki Yamashita, Yi Tang, Tomohiro Namimoto, and Mutsumasa Takahashi. Calculation of T2 Relaxation Time from Ultrafast Single Shot Sequences for Differentiation of Liver Tumors: Comparison of Echo-planar, HASTE, and Spin-echo Sequences, *Radiation Medicine* 2000 18(1):7–14.
27. Youssef Zaim Wadghiri, Jeffrey A. Blind, Xiaohong Duan, Clement Moreno, Xin Yu, Alexandra L. Joyner and Daniel H. Turnbull. Manganese-enhanced magnetic resonance imaging (MEMRI) of mouse brain development. *NMR Biomed.* 2004;17: 613–619.
28. Yves Gossuin, Robert N.Muller. Pierre Gillis, Lionel Bartel. Relaxivities of human liver and spleen ferritin. *Magnetic Resonance Imaging* 2005;23: 1001-1004.

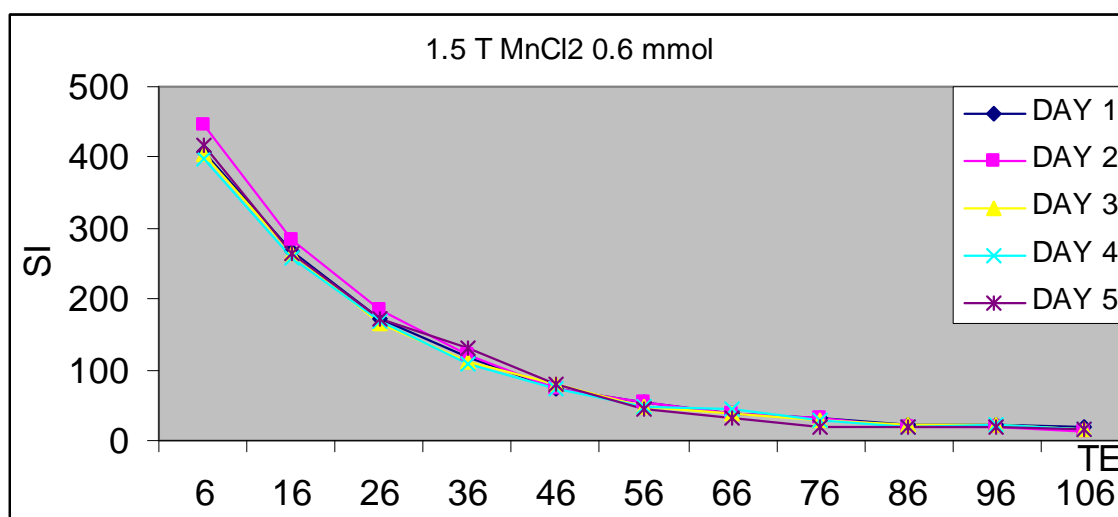
## **APPENDIX**

## APPENDIX A

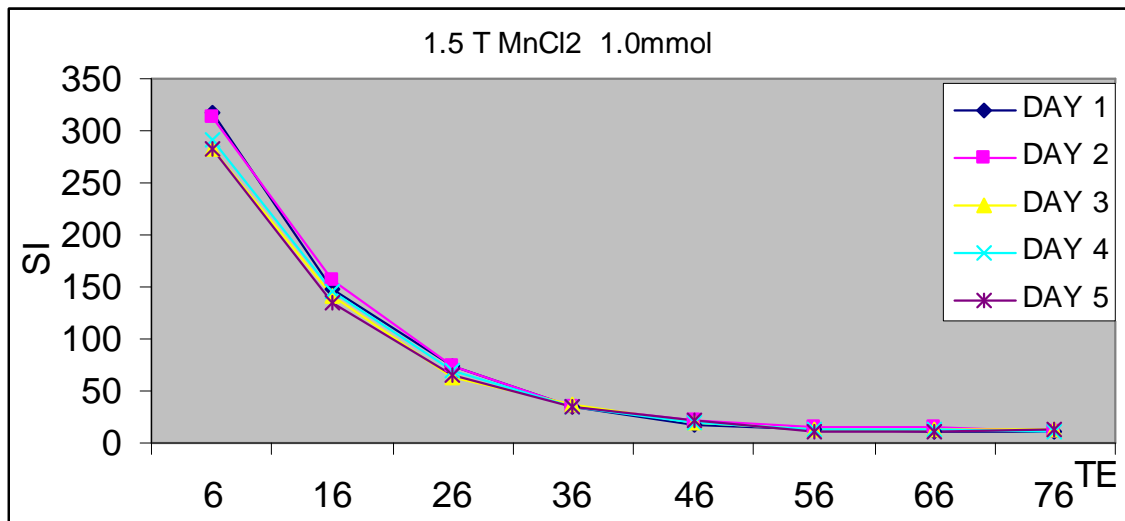
The relationship curve between signal intensities and echo times of manganese chloride solutions concentrations in 1.5 T



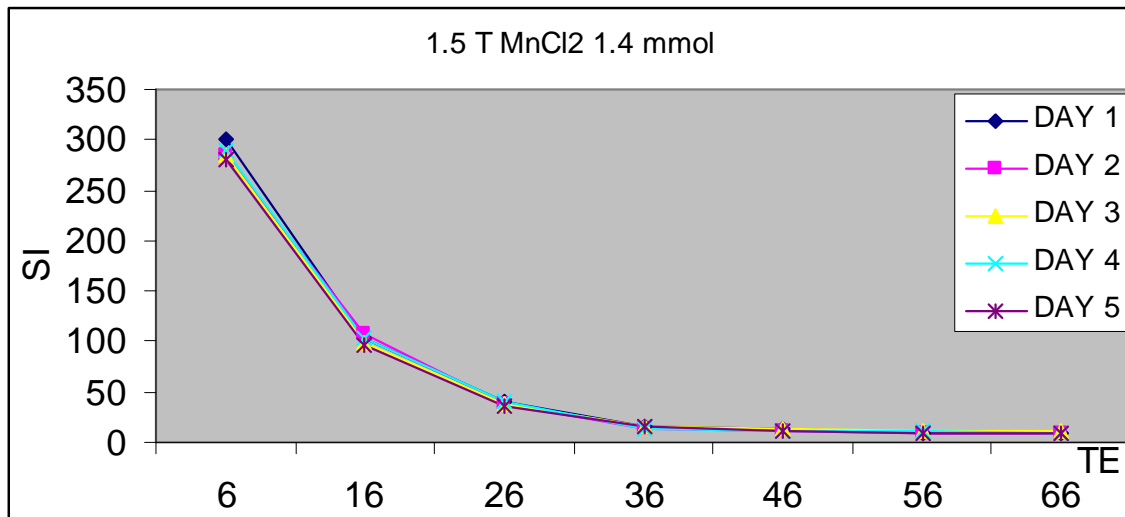
(a)



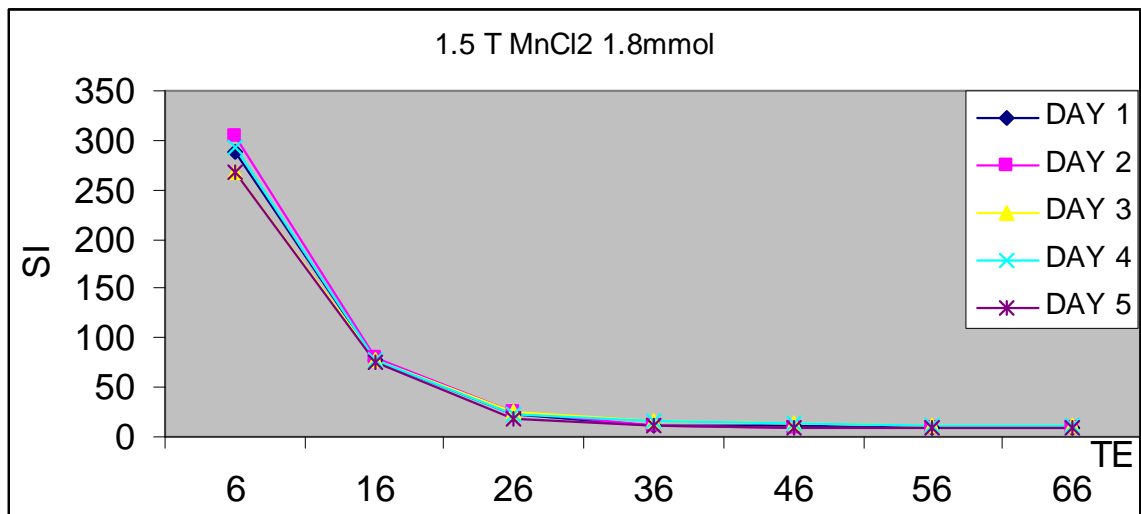
(b)



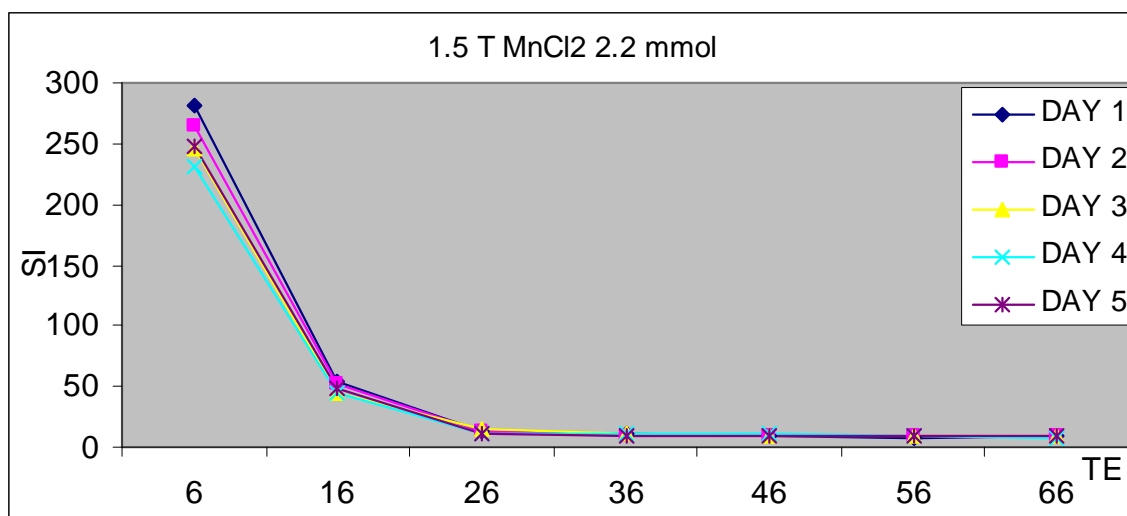
(c)



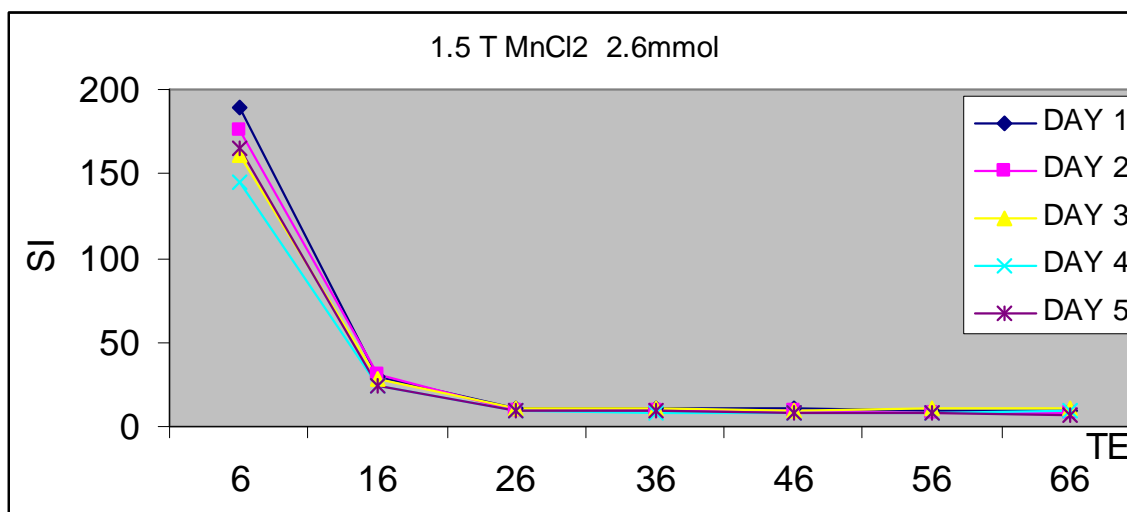
(d)



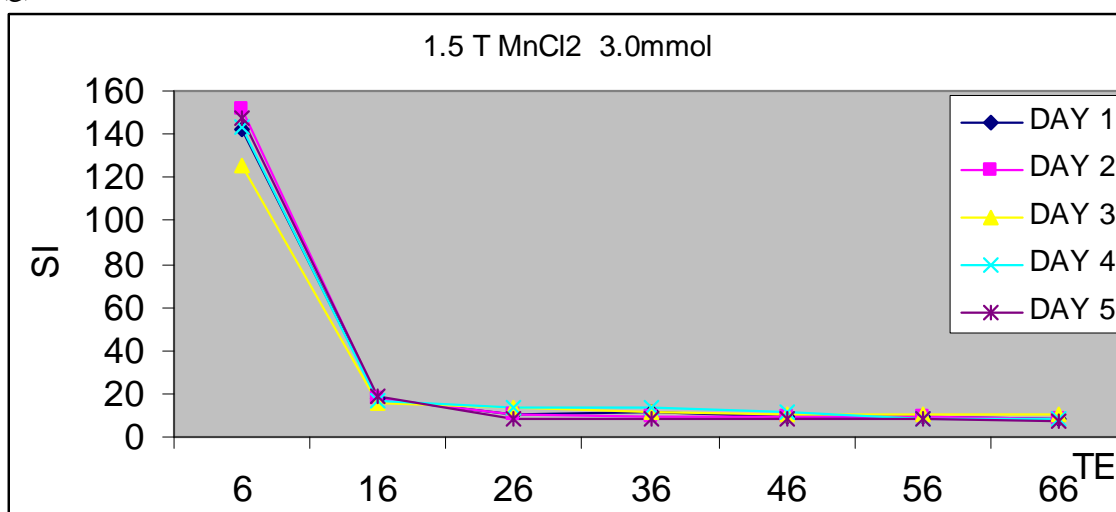
(e)



(f)

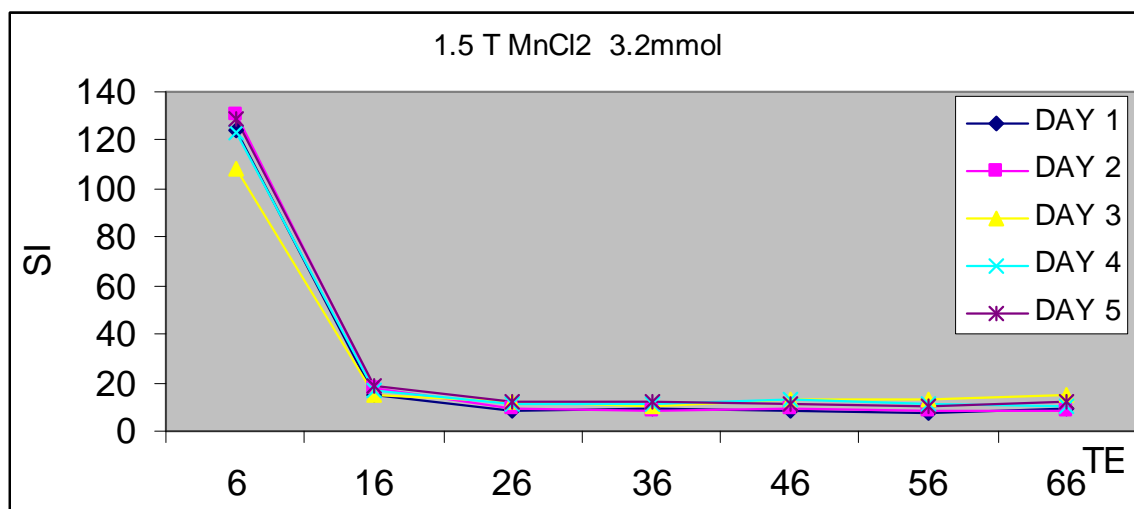


(g)

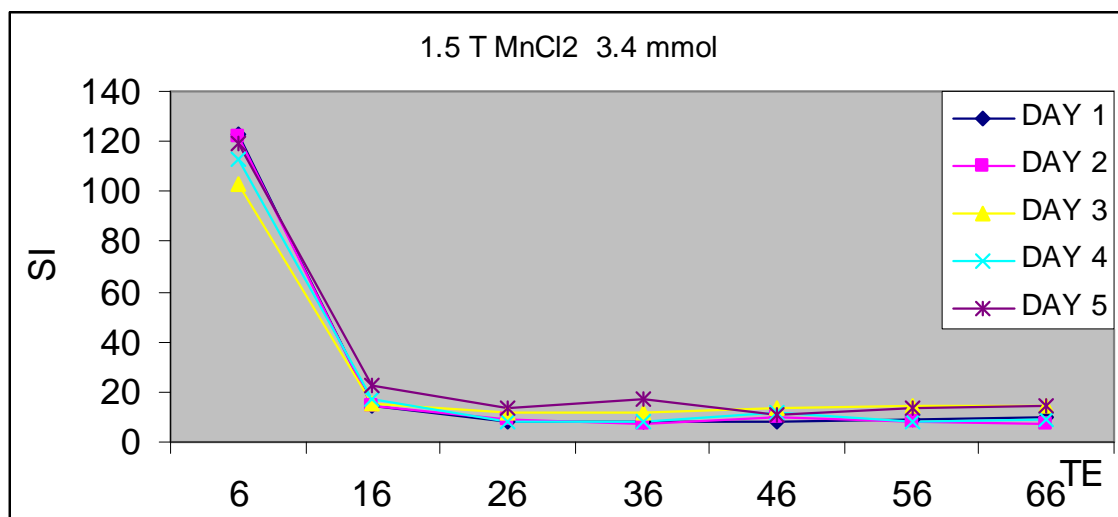


(h)





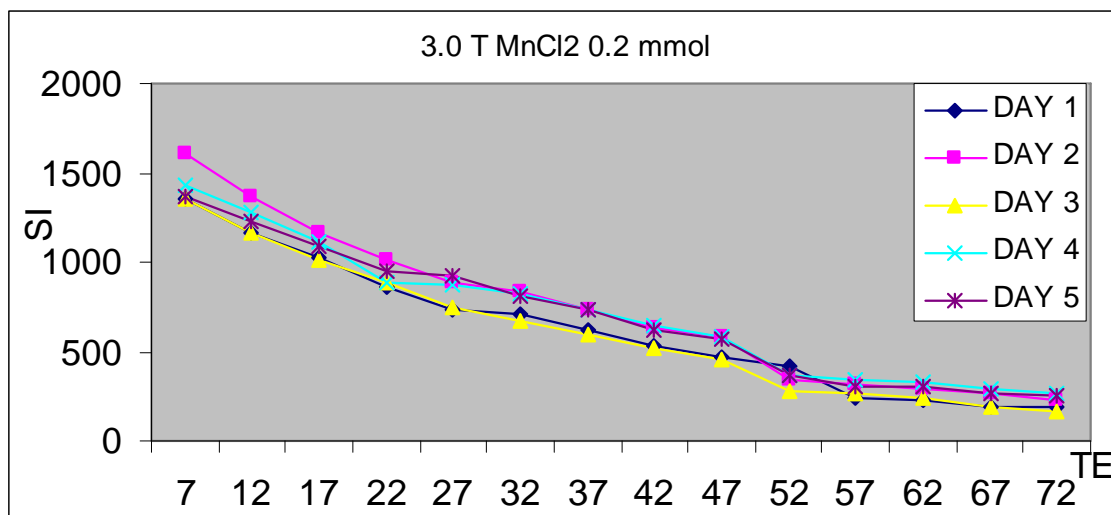
(i)



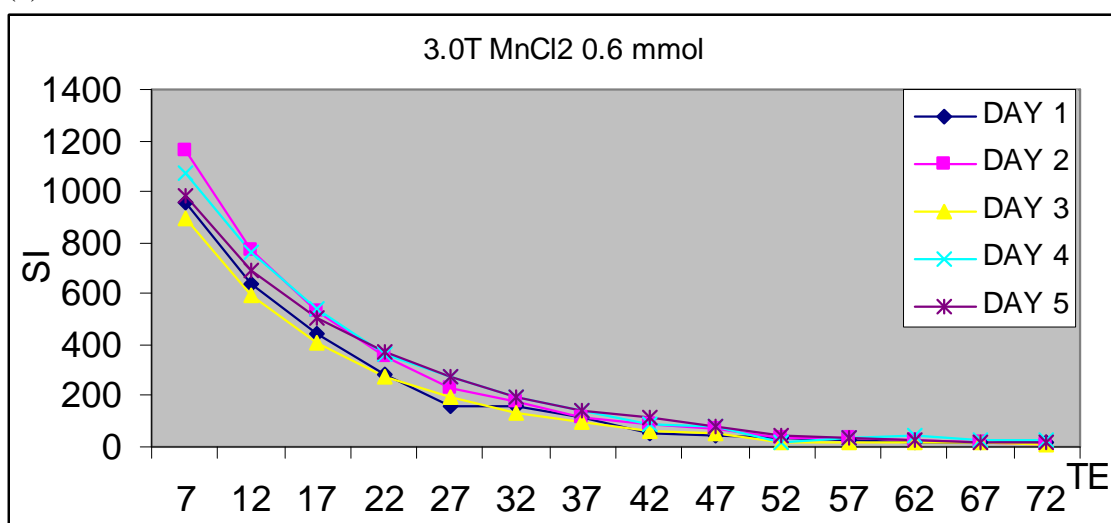
(j)

**Figure. 26.** Plot curve of the relationship between signal intensities and echo times of manganese chloride solutions concentrations in 1.5 T; (a) 0.2 mmol (b) 0.6 mmol (c) 1.0 mmol (d) 1.4 mmol (e) 1.8 mmol (f) 2.2 mmol (g) 2.6 mmol (h) 3.0 mmol (i) 3.2 mmol (j) 3.4 mmol

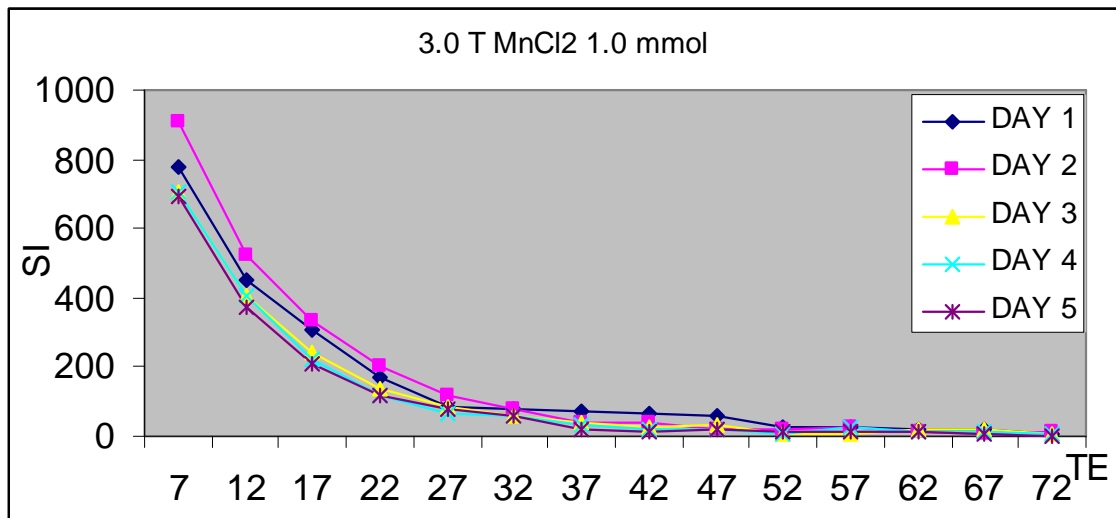
The relationship curve between signal intensities and echo times of manganese chloride solutions concentrations in 3.0 T



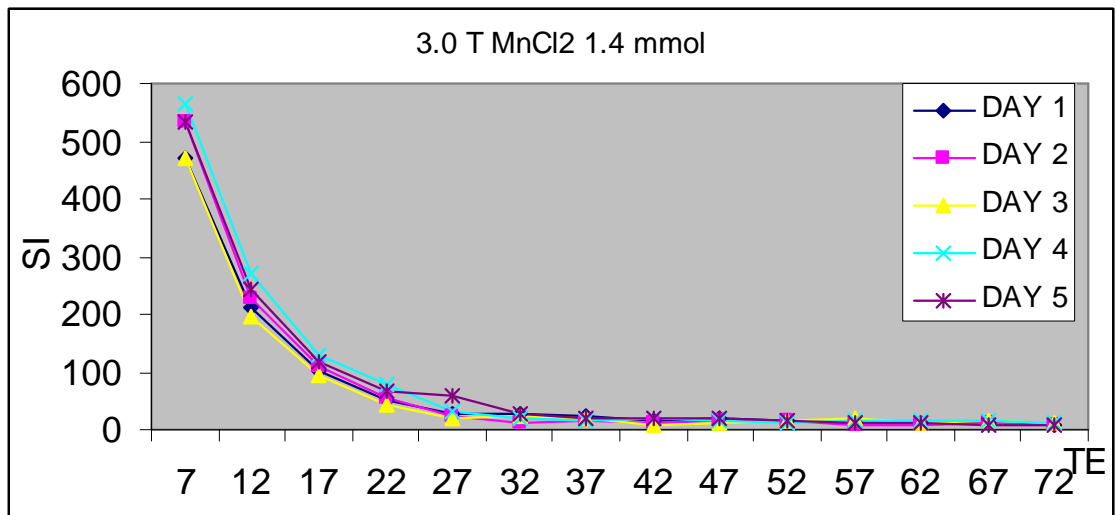
(a)



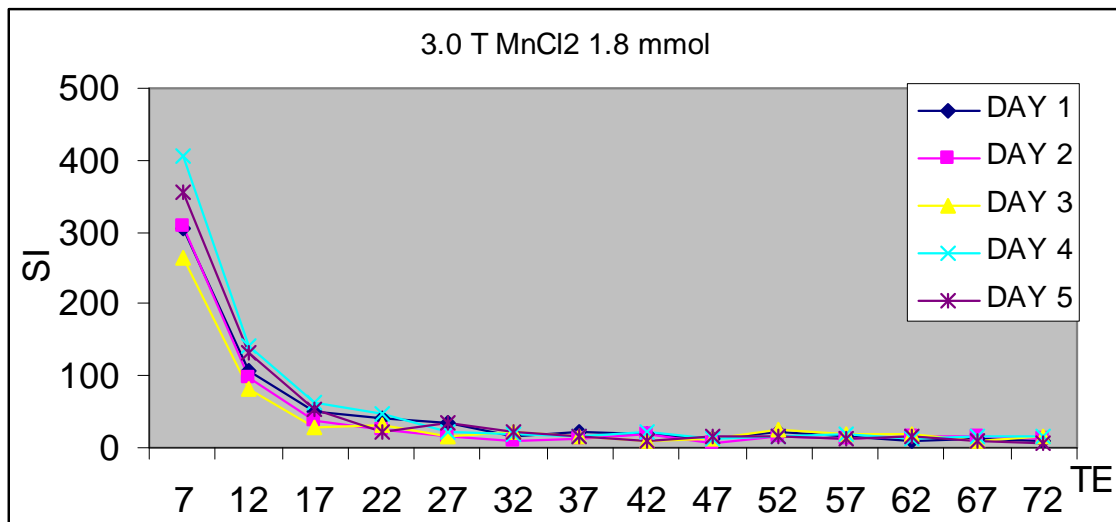
(b)



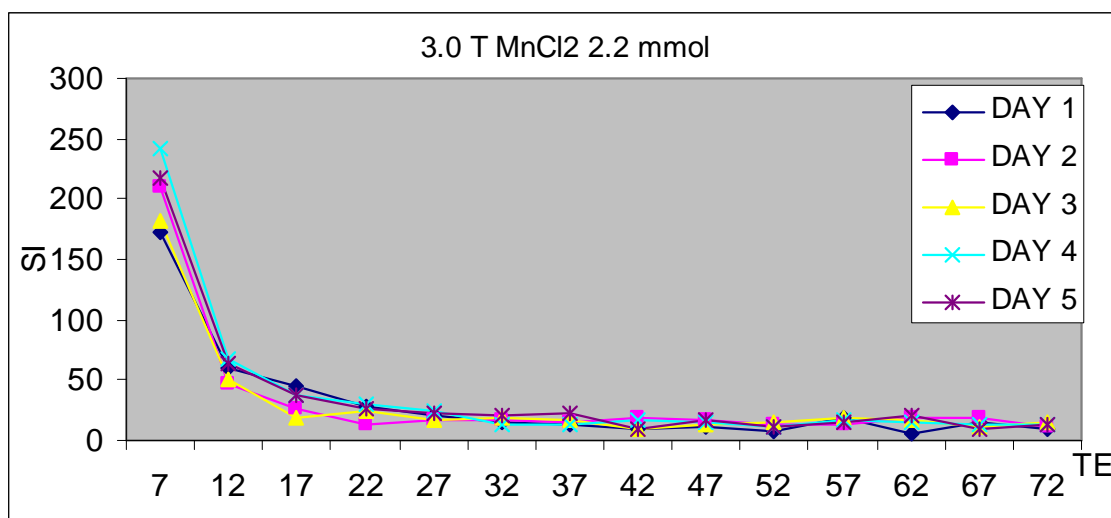
(c)



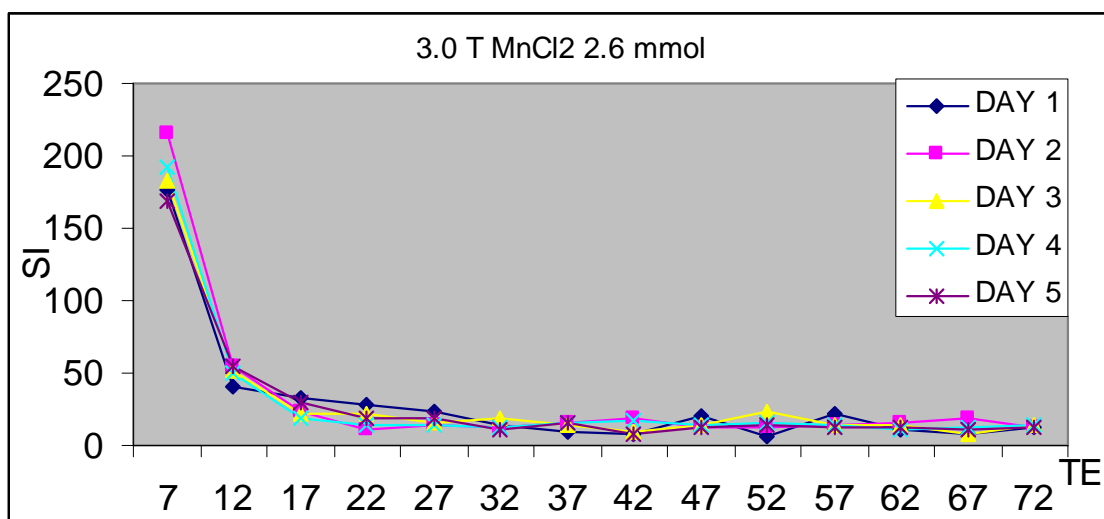
(d)



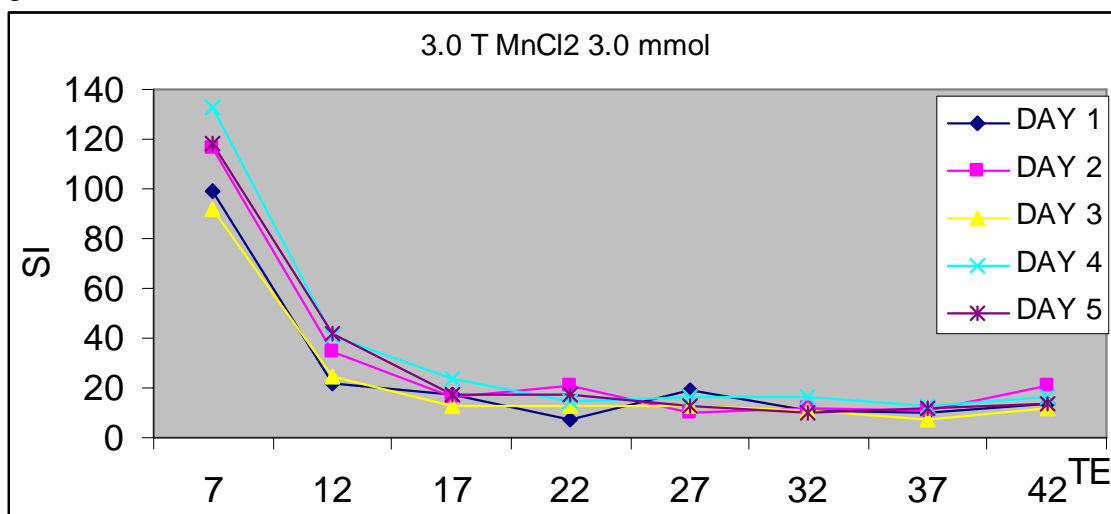
(e)



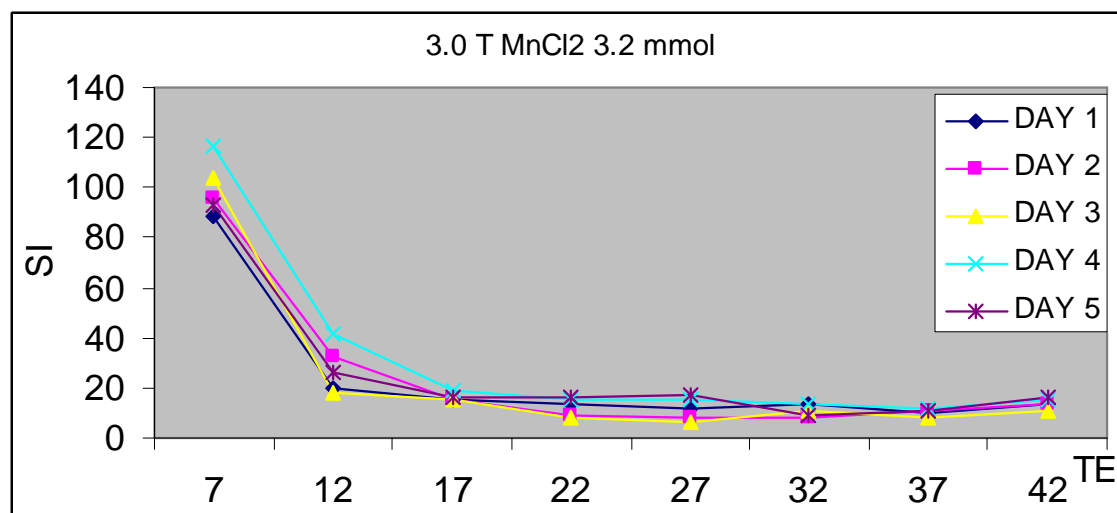
(f)



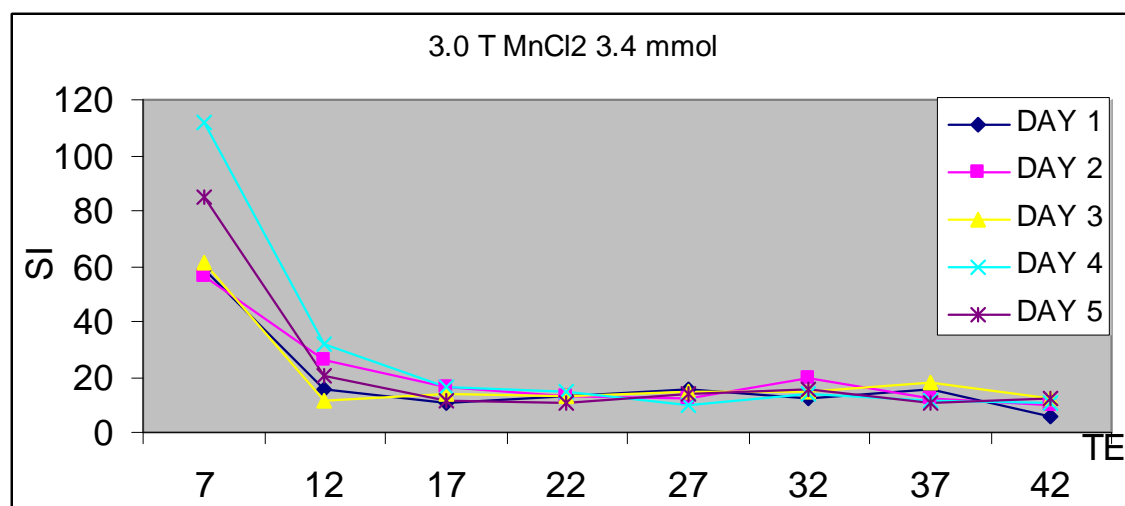
(g)



(h)



(i)



(j)

**Figure. 27.** Plot curve of the relationship between signal intensities and echo times of manganese chloride solutions concentrations in 3.0 T; (a) 0.2 mmol (b) 0.6 mmol (c) 1.0 mmol (d) 1.4 mmol (e) 1.8 mmol (f) 2.2 mmol (g) 2.6 mmol (h) 3.0 mmol (i) 3.2 mmol (j) 3.4 mmol

## BIOGRAPHY

<b>NAME</b>	Miss Watcharee Prasertkulchai
<b>DATE OF BIRTH</b>	4 March 1978
<b>PLACE OF BIRTH</b>	Bangkok
<b>INSTITUTIONS ATTENDED</b>	<p>Mahidol University, 2000:</p> <p>Bachelor of Science ( Radiological Technology)</p> <p>Mahidol University, 2008:</p> <p>Master of Science ( Radiological Technology)</p>
<b>POSITION&amp;OFFICE</b>	<p>270 Ramathibodi Hospital, Bangkok, Thailand</p> <p>Position : Radio technologist</p> <p>Tel. 02-2011251-2</p> <p>E-mail: pomyammy@gmail.com</p>
<b>HOME ADDRESS</b>	<p>79 Charunsanitwong Rd, Bangyeekun, Bangphat, Bangkok, Thailand</p> <p>Tel. 02-4347811</p> <p>E-mail: pomyammy@gmail.com</p>